DEC 1978

Golder Associates
CONSULTING GEOTECHNICAL ENGINEERS

DEC 12 1978

E/78/2639
December 6, 1978

Dr. J.I. Clark, P. Eng.
R.M. Hardy & Associates Ltd.
910, 205 5th Avenue SW
P.O. Box 9327
Bow Valley Square 2
Calgary, Alberta
T2P 2W5

Re: Rehabilitation and Stabilization
Clinton Creek Mine

Dear Jack:

I am enclosing a copy of our report V77016, December 1978, to Cassiar Asbestos Corporation Ltd., which is our response to your report of October 1978 to the Yukon Territory Water Board regarding rehabilitation and stabilization at the Clinton Creek mine site.

As you will see on reading our report, with the exception of your views regarding the Clinton Creek waste dump, we have arrived at different conclusions than are given in parts of the remainder of your report, in particular, in those sections dealing with the seismic analyses which were carried out for the Wolverine Creek tailing pile.

In view of the differences between our respective conclusions, we have asked Cassiar Asbestos Corporation Ltd. not to forward our report to the Yukon Territory Water Board until you have had an opportunity to review both of our positions.

I would be pleased to meet with you at a mutually convenient time to discuss any aspects of the work.

Yours very truly

GOLDER ASSOCIATES

Per: E.B. Fletcher, P. Eng.

EBF:rme
Enclosure

V77016

Golder Associates
CONSULTING GEOTECHNICAL ENGINEERS

REPORT TO
CASSIAR ASBESTOS CORPORATION LTD.
RE
REHABILITATION & STABILIZATION
CLINTON CREEK MINE

CLINTON CREEK YUKON TERRITORY

DISTRIBUTION:

4 copies - Cassiar Asbestos Corporation Ltd.
Vancouver, British Columbia

2 copies - Golder Associates
Vancouver, British Columbia

December 1978

V77016

TABLE OF CONTENTS

		PAGE
1.0	INTRODUCTION	1
2.0	SUMMARY	1
3.0	CLINTON CREEK WASTE PILE	3
4.0	WOLVERINE CREEK TAILING PILE	3
	4.1 General	3
	4.2 Static Stability Analyses	6
	4.2.1 North Lobe	7
	4.2.2 1974 Failure Lobe	10
	4.2.3 Conclusions	11
	4.3 Seismic Stability Analyses	11
	4.3.1 Introduction	11
	4.3.2 Displacements as a Result of Ground Accelerations	12
	4.3.3 Liquefaction	15
	4.3.4 Conclusions	18
5.0	RMHA CONCLUSIONS	18
6.0	RMHA RECOMMENDATIONS	19
7.0	SURFACE TREATMENT OF TAILING PILE	21
	7.1 Wind Erosion	21
	7.2 Water Erosion	22
	7.2.1 Surface Run-off	22
	7.2.2 Percolation of Water into the Tailing Pile	22

1.0 INTRODUCTION

This report is our response to the Yukon Territory Water Board's consultants, R.M. Hardy and Associates Ltd. (RMHA), report and recommendations to the Water Board regarding the rehabilitation and stabilization program carried out by Cassiar Asbestos Corporation Ltd. during closure of mining and milling operations at the Clinton Creek mine site.

2.0 SUMMARY

a) We are in basic agreement with the conclusions reached by RMHA regarding the Clinton Creek waste pile.

b) It is our opinion that monitoring of movements in the Clinton Creek waste pile once every two months will be adequate to evaluate continuing movements in this area, and to determine the required frequency of further monitoring.

c) We are in disagreement with RMHA with respect to the engineering properties of the foundation soils beneath the tailing pile and, consequently, with the mechanism of failure postulated by them. Our findings show that the fluvial lacustrine material, not the weathered argillite, is the principal source of instability beneath the tailing pile.

d) Stability analyses of the tailing pile for the static condition indicate factors of safety against massive downslope failure of 1.3 and 1.6 for the recontoured north lobe and 1974 failure lobe, respectively.

e) Seismic analyses of the recontoured tailing pile indicate that a ground acceleration of 0.15 g, equivalent to an earthquake of magnitude 8-1/4, would cause a downslope displacement of the tailing pile of the order of 12 ft.

f) Seismic analyses indicate that liquefaction of the foundation materials beneath the tailing pile due to seismic loading, and leading to massive downslope failure, is highly improbable.

g) A total of seven new monitors to replace the three monitors removed during recontouring of the north lobe of the tailing pile, and three new monitors to replace the three removed during recontouring of the 1974 failure lobe of the pile, have been established. These, as well as the existing monitors, were surveyed on a weekly basis till November 9, 1978. The average rate of movement of the north lobe of the tailing pile has changed from approximately 0.40 ft./day before recontouring to approximately 0.04 ft./day after recontouring. The rates of movement in the 1974 failure lobe are all of the order of 0.02 ft./day reflecting little change from before recontouring. The consistency of the data was such that we believe that surveys of these installations done every second month will suffice to evaluate the significance of any continuing movements.

h) With respect to the production of a detailed contingency plan for Wolverine Creek in the event of a massive failure of the north lobe of the tailing pile, it is our opinion

that failure leading to further inundation of Wolverine Creek is highly improbable. However, in the event that such a failure does occur, the only reasonable method available for rehabilitation would be to extend the Wolverine Creek bypass channel, constructed at the toe of the 1974 failure lobe, upstream to include materials from subsequent failures. It is impossible to produce a detailed contingency plan beyond this without knowledge of specific post-failure conditions.

i) We are of the opinion that the application of a sealant to the surface of the tailing pile should be considered only if it is found that the naturally forming crust on the tailing pile is breaking down with time.

3.0 CLINTON CREEK WASTE PILE
(reference pages 1 and 2, RMHA report)

We are in basic agreement with the conclusions reached by RMHA regarding treatment of the Clinton Creek waste pile. We feel, however, that monitoring of the movements in the waste pile once every second month, as recommended verbally to you in October 1978, will provide adequate information upon which to base further assessments of these movements.

4.0 WOLVERINE CREEK TAILING PILE
(reference pages 2 to 6, RMHA report).

4.1 General

There are a number of comments and conclusions with which we disagree in this section of RMHA's report. The following comments are

meant to identify these and to point out their implications with regard to their effects when applied to assessments of the stability of the tailing pile.

a) Reference sub-para 1, page 3, RMHA report.

Notwithstanding the generic description of the fluvial lacustrine soils encountered at the site and recorded on the borehole logs, an inspection of the results of six grain size analyses performed on these materials, and included in our report (Golder Associates V77016, July 1978), shows that the samples tested contained 30 to 80 per cent of particles by weight finer than than 0.06 mm (#200 U.S. Standard Sieve). Soils with these grain size distributions will not, as stated in the RMHA report, "... tend to have a relatively high permeability when thawed". The permeabilities of the soils tested will, in fact, be low, and will probably be between 10^{-5} and 10^{-7} cm/sec.

b) Reference sub-para 2, page 3, RMHA report.

i) The R.M. Hardy report states that "... no evidence of ice is recorded in the overburden fluvial lacustrine soil". On page 43 of our report V77016, July 1978, the statement is made that "... The dominant soil type on the upper portion of the slope is a fluvial

lacustrine deposit of silty sandy gravel ... This material was noted during the field investigation to be frost susceptible with as much as 40 per cent, by volume, of ice in the form of lenses". This statement could have been further amplified by stating that these ice lenses were noted in a fresh cut made by bulldozer near the location of borehole 13 (T6). The ice lenses were approximately 1/8 inch thick and were separated by only slightly greater thicknesses of soil. The natural moisture contents of these materials, noted on the borehole log for borehole 13 (T6), are consistent with the visual observations made in the field with regard to ice content.

ii) Sub-paragraph 2 of the RMHA report goes on to say that "... ice was recorded in the weathered argillite and in one test hole a 3 inch lens was recovered". In fact, ice was noted in the weathered argillite at only one location in the Wolverine valley. This was in borehole 18 (DS5) which was made in the bottom of the Wolverine Creek valley. (See Figure 6, V77016 July 1978). Further, an inspection of the grain size analyses performed on samples of the weathered argillite from both the Wolverine and Clinton Creek sites, and included in our July 1978 report, leads to the conclusion that the permeabilities of these

materials are substantially greater than those of the fluvial lacustrine soils at the site.

An additional observational opportunity with regard to the frost susceptibility of the weathered argillite in the Wolverine Creek valley was available in the roadway cut along the west bank of Wolverine Lake below the tailing pile. This cut was made, for the most part, in weathered argillite on May 11 and 12, 1978 for the purpose of moving drilling equipment to the locations of boreholes DS17, 18 and 19 in the Wolverine Creek valley. These materials were noted to drain quickly and without degradation on thawing after their exposure to warm ambient temperatures.

c) Sub-para 3, page 3, RMHA report.

GB.
$\phi_{arg} = 26°$ $\phi_{filoc.} = 29\text{-}32^{30}$ say.
RMH
$\phi_{arg} = 23°$
- Say permeabilities are equal.
- fracture then depend on slip surface & material
- most sensitive when slip surface reaches weathered argillite - $\phi = 25°$ vs. ϕ 30 for flu. lacustrine.

In view of the preceding comments, we disagree with the entirety of sub-para 3 and the first paragraph on page 4 of the RMHA report. In fact, the evidence, as reported in V77016, Section 5.5, July 1978 and amplified in Section 4.2.1 of this report, is quite conclusive with regard to the relative behaviours of the fluvial lacustrine and weathered argillite as foundation soils.

4.2 Static Stability Analyses

Copies of the working drawings used in the analyses of the north lobe of the tailing pile for conditions immediately before and after

recontouring of the tailing pile are included with this report for reference.

The conditions in the tailing pile, the method of analysis, and the parameters and assumptions employed in the analyses are summarized below.

4.2.1 North Lobe

The horizontal and vertical movement data available from observations on surface movement monitors established on the surface of the north lobe of the tailing pile, together with field observations, indicated that a large mass of the tails, with its western boundary just upslope of monitor 26B, was moving en masse downslope at an average rate of approximately 0.40 ft. per day just prior to recontouring (this rate had decreased progressively from a maximum of approximately 0.53 ft. per day recorded during February and March 1978).

The rates of horizontal movement at the locations upslope of this mass varied between 0.01 and 0.015 ft. per day just prior to recontouring. These movements had not changed significantly during the period December 1976 to September 1978 over which observations had been made.

The relationship between the horizontal and vertical movements on the rapidly moving portion of the north lobe indicated that the surface of the pile was moving downslope at angles of approximately 5 degrees steeper than the original ground surface beneath it, which is consistent with the spreading of this portion of the tailing pile as it moved progressively down the slope. The movement data indicated a "stretching" between the

upslope end of this mass and its downslope crest (see Figure 1), with movements near the downslope crest being greater than those further upslope. Conversely, surveyed sections of the tailing pile, as well as field observations, indicated that the wedge of tails between the downslope crest of the pile and its toe was tending to move more slowly with time than the materials upslope of the wedge. The result of this phenomenon was the accumulation of tails at the downslope crest of the pile. This, in turn, caused continuous over-steepening of the front slope of the tailing pile which resulted in the ravelling of tails down the terminal face of the pile. In the period between April 29, 1978 and September 28, 1978, the location of the toe of the pile had moved downslope a distance of approximately 40 ft., an average rate of 0.26 ft. per day, which is substantially less than the rates measured upslope of the crest. Much of this change in the location of the toe of the slope would have been the result of materials ravelling down the face of the pile and accumulating at its toe. Slowing of the toe of the failure mass, and accumulation and over-steepening of the tails upslope of the toe, had not been noted to be occurring on the north lobe of the pile before its toe had reached the steeper natural slope on the west valley wall of Wolverine Creek where little, if any, fluvial lacustrine materials overlie the weathered argillite. The toe wedge could have tended to slow down or stop for only one reason - the foundation soils beneath it were of sufficient strength to resist further downslope movement.

As a result of these observations, the geometry of the failure mass in the north lobe of the tailing pile has been deduced as shown on Figure 1. The soil stratigraphy as it affects the analysis has been

inferred from field observations and is shown in this figure, together with the soil strength parameters as found in the laboratory.

The analyses were done by hand, and, except for the use of non-circular failure surfaces, and the lack of the necessity to choose arbitrary values for the pore pressure ratio, r_u, the analyses are similar to those carried out by RMHA. The following is an outline of the steps used in assessing the stability of the tailing pile under static conditions.

a) The mobilized shear stresses and total normal stresses along the failure surface were calculated and plotted as shown on Figure 2 for both the pre-recontoured and the recontoured tailing pile.

b) The tailing pile was assumed to have a factor of safety of 1.0 before recontouring. Consequently, the mobilized shear stress must, by the definition of the safety factor, be equal to the effective stress times the tangent of the effective angle of internal friction. Using this relationship, the effective normal stress for the pre-recontoured pile was calculated and plotted.

c) At any point along the failure surface, the pore water pressure is equal to the ordinate between the total and effective normal stresses. The pore water pressures along the failure surface after recontouring were assumed to decrease by an amount equal to the reduction in total normal pressure due to recontouring of the pile (i.e. $\overline{B} = 1.0$).

As a result, the effective normal stress along the failure surface is the same before as after recontouring.

d) The factor of safety of the recontoured pile was then calculated by dividing the sum of the mobilized shear stresses into the sum of the effective stresses, both for the recontoured pile, and multiplying this quotient by the angle of internal friction for the soils along the failure surface. The factor of safety for the recontoured north lobe of the tailing pile is estimated to be approximately 1.3.

e) The average pore pressure ratio along that portion of the failure surface over which the tails are in contact with the fluvial lacustrine foundation soils can be calculated by dividing the sum of the pore water pressures by the sum of the total normal pressures and dividing this quotient by the square of the cosine of the base angle of the failure mass, i.e. $r_u = u/\sigma/\cos^2\theta$. The values of r_u for the north lobe of the tailing pile were found to be 0.53 and 0.39 for conditions before and after recontouring, respectively.

f) The results of the analyses for the conditions immediately before and after recontouring of the north lobe of the tailing pile, are summarized on Figure 2.

4.2.2 1974 Failure Lobe

As shown in our report, V77016, July 1978, the movements in the 1974 failure lobe of the tailing pile were much slower than those in the

north lobe. Due to the requirements of Wolverine Creek channel realignment and grading, this segment of the tailing pile was also recontoured. Analyses of the failure lobe for conditions, before and after recontouring, and using the same techniques described for the north lobe of the tailing pile were carried out and the factor of safety after recontouring has been estimated to be approximately 1.6.

4.2.3 Conclusions

We believe that the observations, assumptions, and analytical techniques that we have applied are appropriate to a realistic assessment of the behaviour of the tailing pile under static loading conditions.

4.3 Seismic Stability Analyses

4.3.1 Introduction

The use of a pseudo-static analysis, as carried out by RMHA, to evaluate the response of a soil mass to earthquake loading applies the following assumptions and effective net changes to a static analysis of the soil mass.

a) the earthquake force, k(g), which is being imposed upon the slope is assumed to be continuous (not cyclic), to be acting in the plane of the section being analyzed, and to be acting only in the downslope direction.

b) the entire geometry of the slope is effectively steepened by an amount exactly equal to the arctangent of the earthquake factor being used.

c) the weight of every element of the failure mass is effectively increased by a factor equal to $\sqrt{1 + k^2}$.

The configuration which results from these changes is then effectively subjected to a static analysis. In simple terms, this type of analysis states that every slope which consists of cohesionless materials, such as the tailing pile and its foundation soils, and which is subjected to earthquake loading, will ultimately flatten to an angle equal to its static angle of repose minus the arctangent of the earthquake factor applied.

There are, in fact, two separate and distinct potential effects caused by the imposition of earthquake forces on natural or man-made slopes. The first of these is displacement as a direct result of ground accelerations, and the second is liquefaction of the slope or its foundation soils as a result of ground shaking. The pseudo-static analysis does not account for these effects and, consequently, is generally an inappropriate method of analysis when applied to slope stability problems. The displacement and liquefaction phenomena associated with earthquakes are dealt with in the following paragraphs.

4.3.2 Displacements as a Result of Ground Accelerations

In a slope of relatively uniform density, such as the tailing pile, subjected to a reasonably uniform acceleration throughout its height, experimental evidence (Goodman and Seed (1966) and Makdisi and Seed

(1978)) suggests that failure occurs by mass sliding of a thin surface zone. During acceleration of the earthquake, inertia forces may induce momentary instability of this mass causing it to slide downhill. However, before any appreciable movements occur, the direction of ground acceleration is reversed and the motion of the surface layer is arrested, only to be started again during the following acceleration cycle. The overall effect is a progressive displacement causing flattening of the slope at its toe and settlement at its crest. If the initial inclination of the slope is less than the friction angle, movement can only occur when the inertia forces induce temporary instability, and no further displacement will occur when the ground motion has ceased. Techniques to calculate earthquake induced displacements have been developed by Goodman and Seed (1966), and Makdisi and Seed (1978). Neither of these techniques rely on the pseudo-static method of analysis to arrive at estimates of final displacements.

a) Goodman and Seed (1966): The analytical technique assumes that the friction angle and shear strength intercept decrease with shear deformation and that each successive acceleration pulse produces a corresponding displacement of the slope. Figure 3 illustrates this phenomenon. Numerical integration can be used to calculate displacement from an expression for the velocity or, alternatively, there is a simplified expression for displacement.

b) Makdisi and Seed (1978): There are three steps in the calculation of displacement by this method. These are:-

i) Static analyses are carried out to determine the horizontal acceleration ("yield acceleration"), $k_y(g)$, required to cause failure of the slope (see Figure 4).

ii) The earthquake induced accelerations, k_{max}, in the slope can be calculated by using programs such as SHAKE, QUAD-4, or by using a simplified procedure described by Makdisi and Seed (1978), or resort can be made to statistical data such as that provided to RMHA by Pacific Geoscience Centre.

iii) Design charts have been drawn up using numerical integration which can be used to determine displacement from the quantities found in (a) and (b) (see Figure 5).

Using this second technique with selected earthquake factors, displacements of the tailing pile have been estimated and are given in the following table.

Earthquake Intensity (Modified Mercalli)	Mean Number of Cycles N_c	Earthquake Factor $k_{max}(g)$	Yield Accel. of Slope $k_y(g)$ (see Fig 4)	$\frac{k_y}{k_{max}}$	Est'd Cumulative Downslope Displacement of Tails (see Fig 5)
6.0	5	0.03 g	0.04 g	1.33	0.0 ft.
7.0	10	0.06 g	0.04 g	0.67	0.3 ft.
7.75	17	0.10 g	0.04 g	0.40	3.5 ft.
8.25	23	0.15 g	0.04 g	0.27	12 ft.

The calculated displacements seem small in view of widespread notions of the effects of earthquakes on slopes. They are, however, consistent with observed displacements due to earthquake occurrences (see Seed et al (1973)).

4.3.3 Liquefaction

The second effect of the imposition of earthquake forces on a cohesionless soil mass is the possible liquefaction of the material. For the case being considered, the tails themselves are essentially free of water and, therefore, not susceptible to liquefaction. The only effect on the tailing pile, exclusive of its foundation soils, due to seismic loading, will be lateral displacement as discussed in the previous paragraphs. However, the soils underlying the tailing pile are saturated when they are thawed and may be susceptible to liquefaction. Obviously, if widespread liquefaction were to occur in the foundation soils, the tailing pile would move downslope, possibly engulfing Wolverine Creek.

The evaluation of a soils susceptibility to liquefaction under seismic loading is a difficult process and many technical papers and reports have been published on the subject. Seed et al (1971, 1973, 1975a), b) and c), 1976, 1978 and others) have developed the most widely accepted techniques for assessing liquefaction potential. Finn et al (1978), have published a paper concerned with the liquefaction of sandwiched thawed layers in frozen soils which is of direct concern to the conditions in the foundation soils beneath the tailing pile. The work reported on by these authors is used to evaluate the liquefaction potential of the tailing pile as outlined in the following paragraphs.

The techniques proposed by Seed et al, vary from the use of highly sophisticated laboratory and field measurements and mathematical analyses to obtain information pertinent to the liquefaction problem, to the use of simple charts upon which to base an assessment of liquefaction potential. These are found principally in Seed et al (1971, 1973, 1975a), b), and c), 1976, and 1978). The procedures from Seed et al (1971a)), adjusted for sloping ground, have been used for the analysis included with this document. The results of the analysis are shown on Figure 6, and are summarized in the following table.

How is the F.S. against liquefaction defined?

Earthquake Intensity (Modified Mercalli)	Mean Number of Cycles N_c	Earthquake Factor k_{max}(g)	Factor of Safety Against Liquefaction		
			Initial $r_u = 0.3$	Initial $r_u = 0.4$	Initial $r_u = 0.5$
6.0	5	0.03 g	1.43	1.21	1.05
7.0	10	0.06 g	1.38	1.16	0.95
7.75	17	0.10 g	1.29	1.07	0.88
8.25	23	0.15 g	1.19	1.0	0.81

NOTE: The pore pressure ratio, r_u, for the recontoured tailing pile has been estimated to be 0.38. This value will decrease slowly with time as temperature equilibrium is achieved in the foundation soils and as consolidation of these materials continues. Consequently, the factor of safety with regard to liquefaction potential will increase with time.

Whereas the resistance to liquefaction of the foundation soils, according to this analysis, is good, it does not preclude the probability

that pore pressures will increase during earthquake loading. Increases in pore water pressures will occur only on a cyclic basis since the low permeabilities of the foundation soils will not allow physical redistribution of water during the short time periods of earthquake stress application. The increases in pore pressure are due to the temporary imposition of these external forces. In other words, increases in r_u will last only as long as the earthquake forces are applied. Consequently, we have in this particular case, a situation where the slope may begin to fail, only to be arrested when the pore pressures again drop below the critical values with the abatement of seismic forces.

The paper by Finn et al (1978), is particularly germane to considerations of the liquefaction potential of the tailing pile foundation soils under earthquake loading. In the work reported upon in this publication, the authors applied dynamic analyses to soils with permeabilities of 0.01, 0.1 and 1.0 cm/sec., relative densities of 45 and 63 per cent, and using the first 10 seconds of the acceleration component of the El Centro earthquake (1940) scaled to a maximum acceleration of 0.08 g. The results of these analyses "... provide a clear picture of what goes on in the saturated sandwich layer during an earthquake. The earthquake motions generate pressure gradients in the pore water, and under summer conditions, drainage can occur through the surface of the layer. The amount of drainage depends on the permeability of the layer. If the permeability of the layer is less than 0.1 cm/sec., the effect of drainage on pore pressures during an earthquake is negligible, and it makes little difference whether the surface layer is frozen or not, or whether the analysis is carried out in terms of effective or total stress", (Finn et al (1978)).

It seems reasonable to extrapolate these conclusions to the situation that exists beneath the tailing pile. The permeabilities of the fluvial lacustrine deposit are at least 4 orders of magnitude less than the critical value deduced by Finn et al, and the values in the weathered argillite are estimated to be at least 2 orders of magnitude less than this critical value. These factors should account for the higher values of ground acceleration of 0.1 g and 0.15 g proposed by RMHA as appropriate for application to the Clinton Creek area.

In view of the considerations outlined in the attached analysis and in the preceding paragraphs, it is our opinion that the foundation soils and the tailing pile have almost no potential for liquefaction leading to massive failure of the tailing pile.

4.3.4 Conclusions

To conclude our considerations of the effects of earthquake loading on the Wolverine Creek tailing pile, it is our opinion that the most serious effect in terms of downslope movement of the pile would involve a downslope displacement of the pile of the order of 12 ft. due to the imposition of ground waves consistent with a magnitude 8-1/4 earthquake (k_{max} = 0.15). The probability of such an event occurring in a given year is, according to an extrapolation of the statistical analysis provided by the Pacific Geoscience Centre, approximately 0.004.

5.0 RMHA CONCLUSIONS
(reference pages 7 and 8, RMHA report)

The preceding sections should suffice as our response to the conclusions arrived at in the RMHA report.

6.0 RMHA RECOMMENDATIONS
(reference page 7, RMHA report).

a) Reference sub-para 1, page 7, RMHA report)

In view of the findings presented in our report V77016, July 1978, and in this document, it is our opinion that a failure in the tailing pile leading to further inundation of Wolverine Creek is highly improbable. However, in the event that such a failure does occur, the only reasonable method available for rehabilitation would be to extend the Wolverine Creek by-pass channel, constructed at the toe of the 1974 failure lobe, upstream to include materials from subsequent failures. It is impossible to produce a detailed contingency plan beyond this without knowledge of specific post-failure conditions.

b) Reference sub-para 2, page 7, RMHA report

It is our opinion that monitoring of movements in the Clinton Creek waste pile once every two months, as recommended previously, will be adequate to evaluate continuing movements in this area, and to determine the required frequency for further monitoring.

c) Reference sub-para 3, page 7, RMHA report

A total of seven new monitors to replace the three monitors removed during recontouring of the north lobe of the tailing

pile, and three new monitors to replace the three removed during recontouring of the 1974 failure lobe of the pile, have been established according to our recommendations made prior to recontouring. Their locations are shown on Figure 7. These monitors were surveyed on a weekly basis till November 9, 1978. The average rate of movement of the north lobe of the tailing pile has changed from approximately 0.40 ft./day before recontouring to approximately 0.04 ft./day after recontouring. The rates of movement in the 1974 failure lobe are all of the order of 0.02 ft./day, reflecting little immediate change as a result of recontouring. The consistency of the data was such that we believe that surveys of these installations, as well as the remaining undisturbed monitors on the tailing pile, done every second month, will suffice to evaluate the significance of any continuing movements.

d) Reference sub-para 4, page 7, RMHA report

Sections of the recontoured tailing pile were surveyed after recontouring was completed. The sections were taken along coordinate lines 113400 N and 113600 N (1974 failure lobe) and 114350 N, 114500 N and 114650 N (north lobe). It is our opinion that these surveys provide an adequate topographic view of the tailing pile in its reconstructed state. A map of the recontoured tailing pile is included as Figure 7.

e) Reference sub-para 5, page 7, RMHA report

Stability analyses of the tailing pile were done immediately before recontouring began, using updated survey data so that the recontouring plan could be finalized, and again immediately following recontouring using survey data taken on the recontoured surface. The results of this work were discussed earlier in this document.

7.0 SURFACE TREATMENT OF TAILING PILE (reference RMHA letter, July 31, 1978)

We remain of the opinion that sealing of the surface of the tailing pile to control the transport of fines by wind or water is unnecessary.

7.1 Wind Erosion

It is our opinion that nearly all of the wind blown dust originated from the belt conveyor system as the tails were transported from the mill to the tailing pile. With the closure of the mill, this source has been eliminated.

As a result of the formation of a natural crust on the surface of the pile, wind erosion of fines from the pile will be minimal except in localized areas where cracking may occur as a result of continuing subsidence of the pile. Consequently, unless there is evidence to show that wind blown fines from the surface of the pile are a hazard to the environment, or that the naturally forming crust will break down with time,

the installation of an artificial surface sealant will not appreciably change the existing conditions. Even the best sealants available will eventually break down as a result of exposure to weathering, ultra violet light, and successive wetting and drying and freezing and thawing cycles.

- C.A.C. to investigate & compare cost & effectiveness of sealants vs re-vegetation.

7.2 Water Erosion

7.2.1 Surface Run-off

There is no evidence that surface water presently collects and runs off the surface of the tailing pile causing erosion and transport of fines into Wolverine Creek.

Placing of a surface sealant on the tailing pile would result in efficient removal of rainfall and snowmelt from its surface provided that the pile was shaped so that no ponding could occur and provided that the surface sealant maintained its integrity. However, the application of a surface sealant could precipitate new problems in terms of the formation of erosional features in the terrain downslope of the tailing pile or, if the surface seal deteriorated or cracked for any reason, particularly in depressions on the surface of the pile, erosional features could form in these locations causing the transport of fines directly into Wolverine Creek.

7.2.2 Percolation of Water into the Tailing Pile

The problem of the downward percolation of water and water-borne asbestos fibre through the tailing pile was raised in the RMHA July 31, 1978 letter. The amount of water that enters the pile through its surface

and travels downward and into the foundation soils is determined by local climatic conditions as well as by the porosity and water retention characteristics of the tails. We have not analyzed this problem in terms of detailed assessments of the variables. However, observations were made in cuts up to 65 ft. in height in the 1974 failure lobe during its recontouring in August and September 1978. The materials were found to be basically dry throughout the depths of these cuts which suggest that nearly all of the precipitation which falls on the tailing pile is ultimately accommodated by evaporation. Consequently, we are of the opinion that the problem of water-borne asbestos fibre entering the ground water system by the downward percolation of water through the tailing pile is of debatable concern.

Yours very truly

GOLDER ASSOCIATES

Per: D.B. Campbell, P. Eng.

E.B. Fletcher, P. Eng.

DBC/EBF:rme

V77016

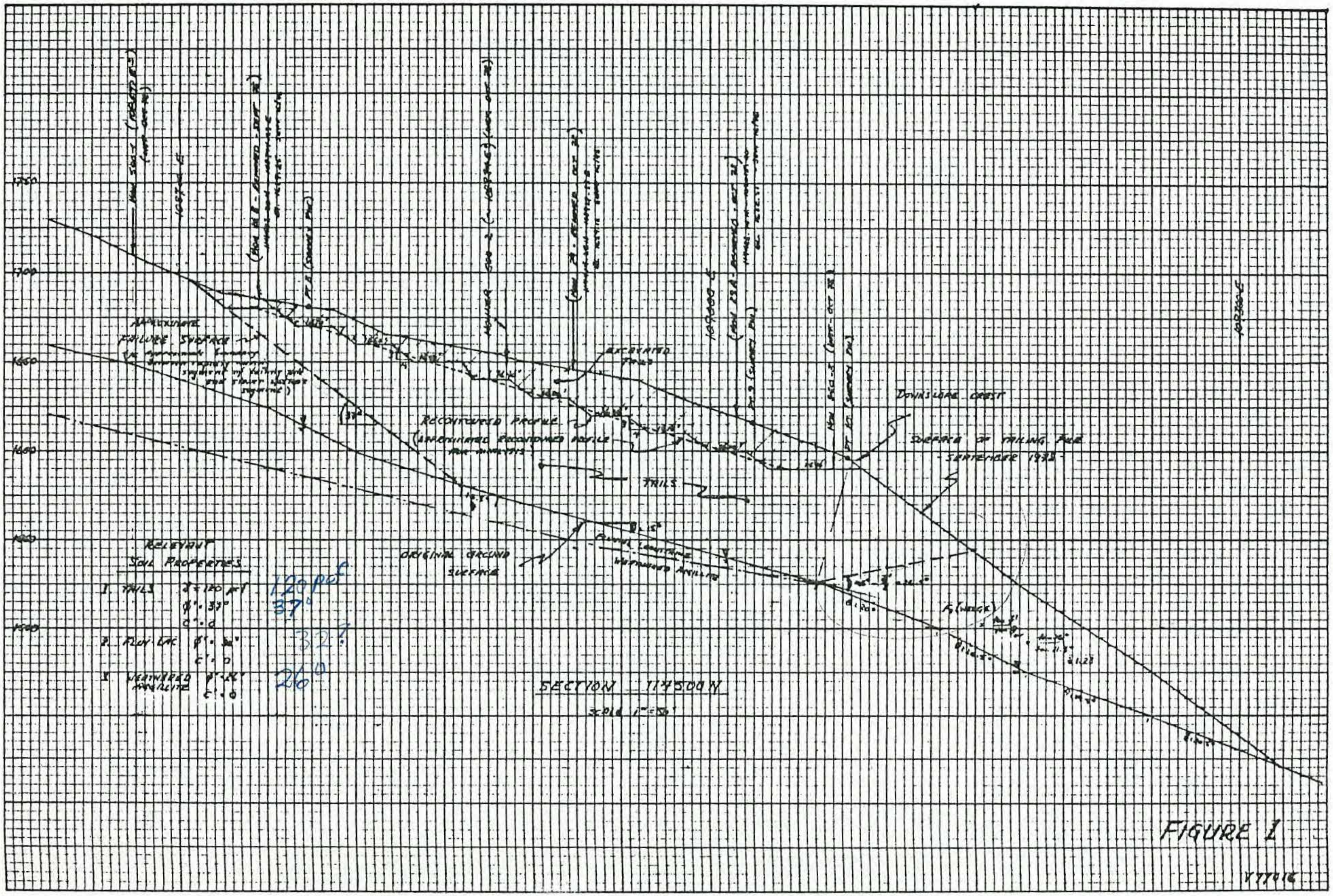

BIBLIOGRAPHY

1. Finn, W.D.L., Yong, R.N. and Lee, K.W. (1978), "Liquefaction of Thawed Layers in Frozen Soils", Journal of the Geotechnical Engineering Division, ASCE, Vol. 104, No. GT10, Oct., pp. 1234 - 1255.

2. Golder Geotechnical Consultants Ltd. (1978), "Report to Cassiar Asbestos Corporation Ltd. re Mine Waste Dump and Tailing Pile Clinton Creek Operations", July.

3. Goodman, R.E., and Seed, H.B. (1966), "Earthquake-Induced Displacements in Sand Embankments", Journal of the Soil Mechanics and Foundations Division, ASCE, Vol. 92, No. SM2, March, pp. 125 - 146.

4. Hardy, R.M., and Associates Ltd. (1978), "Report to the Yukon Territory Water Board re Stabilization and Reclamation Clinton Creek Mine", Oct.

5. Makdisi, F.I., and Seed, H.B. (1978), "Simplified Procedure for Estimating Dam and Embankment Earthquake - Induced Deformations", Journal of the Geotechnical Engineering Division, ASCE, Vol. 104, No. GT7, July, pp. 849 - 867.

6. Martin, G.R., Finn, W.D.L., and Seed, H.B. (1975a)), "Fundamentals of Liquefaction under Cyclic Loading", Journal of the Geotechnical Engineering Division, ASCE, Vol. 101, No. GT5, pp. 423 - 438.

7. Seed, H. Bolton (1976), "Some Aspects of Sand Liquefaction Under Cyclic Loading", Proceedings, Conferences on Behaviour of Off-Shore Structures, The Norwegian Institute of Technology, Norway.

8. Seed, H. Bolton, Arango, I., and Chan, Clarence K. (1975b)), "Evaluation of Soil Liquefaction Potential During Earthquakes", Report No. EERC 75-28, Earthquake Engineering Research Center, University of California, Berkeley, October.

9. Seed, H. Bolton and Idriss, I.M. (1971), "Simplified Procedure for Evaluating Soil Liquefaction Potential", Journal of the Soil Mechanics and Foundations Division, ASCE, Vol. 97, No. SM9, pp. 1249 - 1273.

10. Seed, H.B., Lee, K.L., Idriss, I.M., Makdisi, F. (1973), "Analysis of the Slides in the San Fernando Dams During the Earthquake of February 9, 1971", Report No. EERC 73-2, Earthquake Engineering Research Centre, University of California, Berkeley, June.

11. Seed, H. Bolton, Mori, Kenji and Chan, Clarence K. (1975c)), "Influence of Seismic History on the Liquefaction Characteristics of Sands", Report No. EERC 75-25, Earthquake Engineering Research Center, University of California, Berkeley, August.

INTEGRATION OF ACCELEROGRAMS TO DETERMINE DOWNSLOPE DISPLACEMENTS.

Figure 3

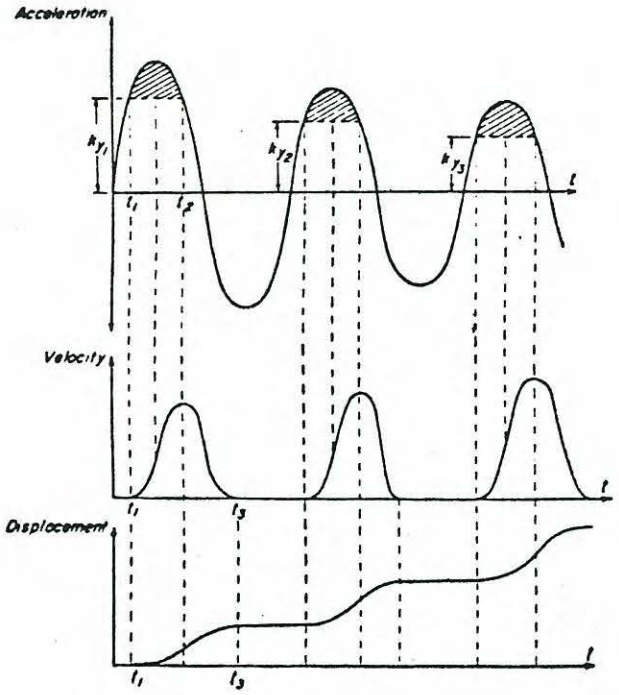

(REF.: Goodman & Seed (1966))

Project No. 177016 Drawn: EG Rev'd: [illegible] Date: Dec/28

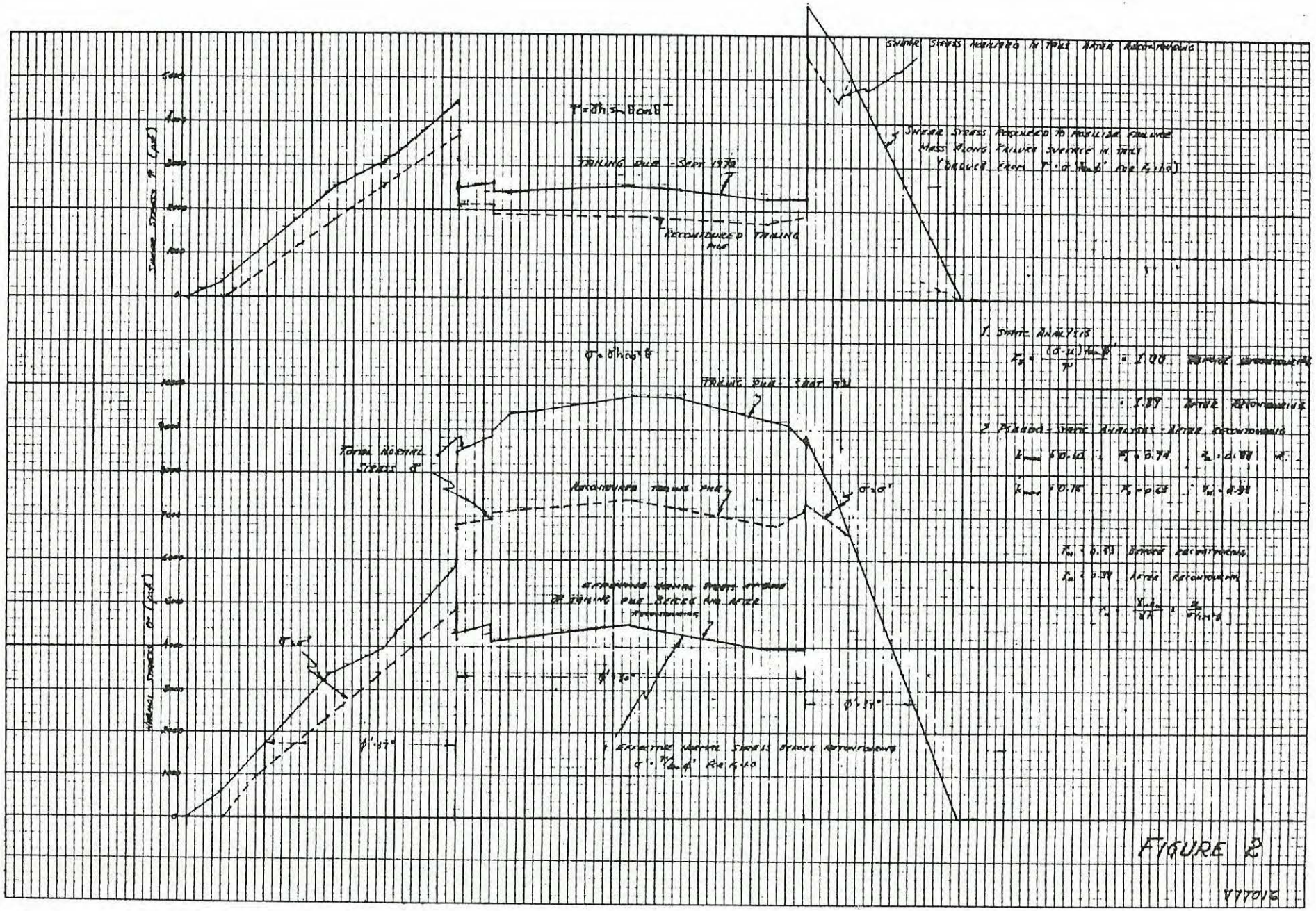
FIGURE 2

DETERMINATION OF YIELD ACCELERATION FOR NORTH LOBE — Figure 4

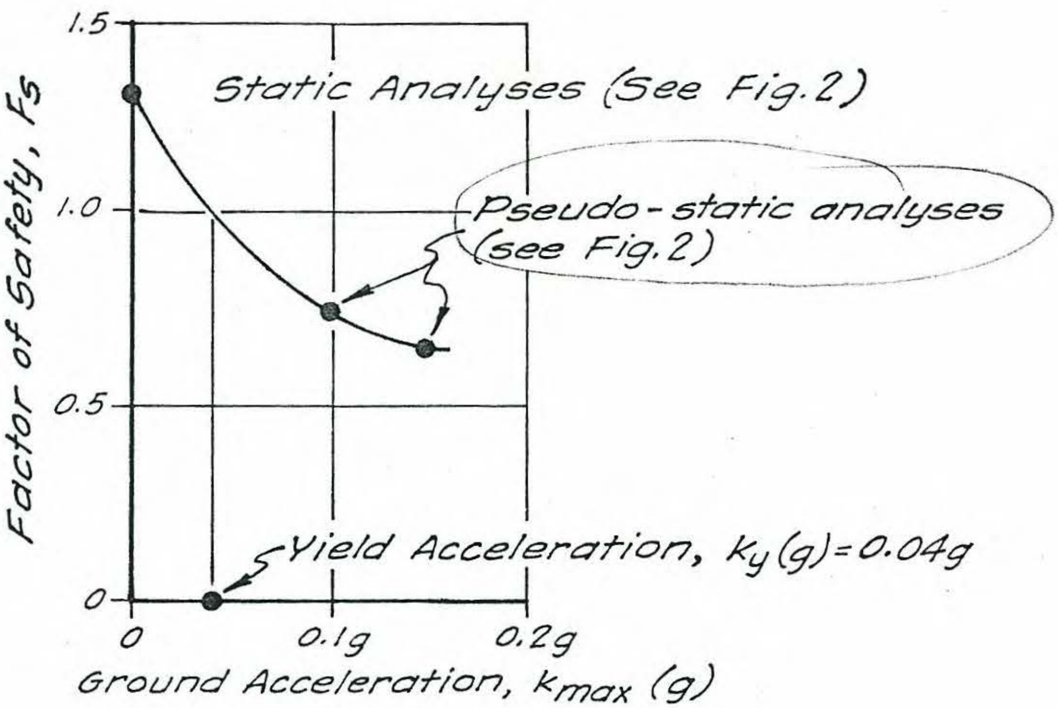

Project No V77016 Drawn EG Reviewed [illegible] Date Dec. '78

RELATIONSHIP BETWEEN ky/kmax AND TOTAL HORIZONTAL DISPLACEMENT

Figure 5

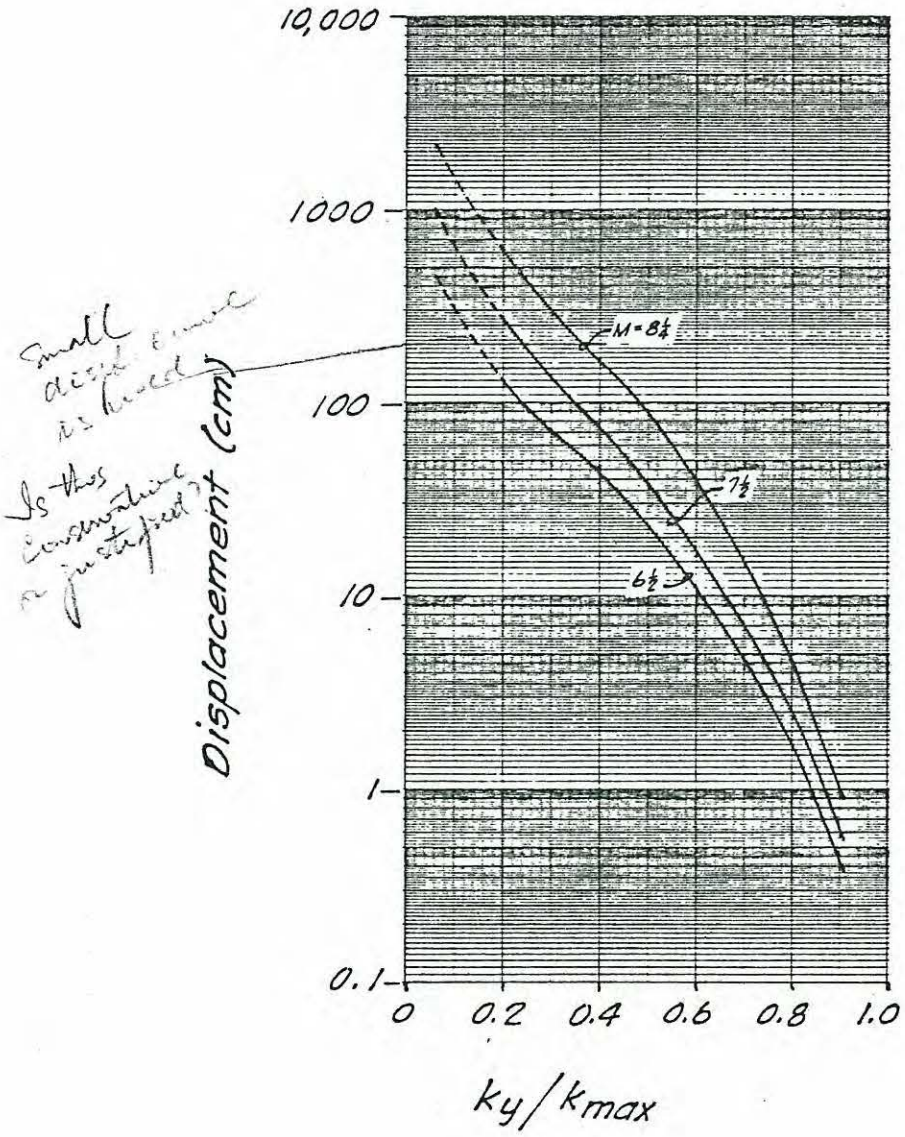

(REF.: Makdisi & Seed (1978))

M = magnitude

Project No. 17-7016. Drawn: Iq Reviewed: SB Date Dec/18.

INDUCED CYCLIC SHEAR STRESS VS MAXIMUM GROUND ACCELERATION.

Figure 6

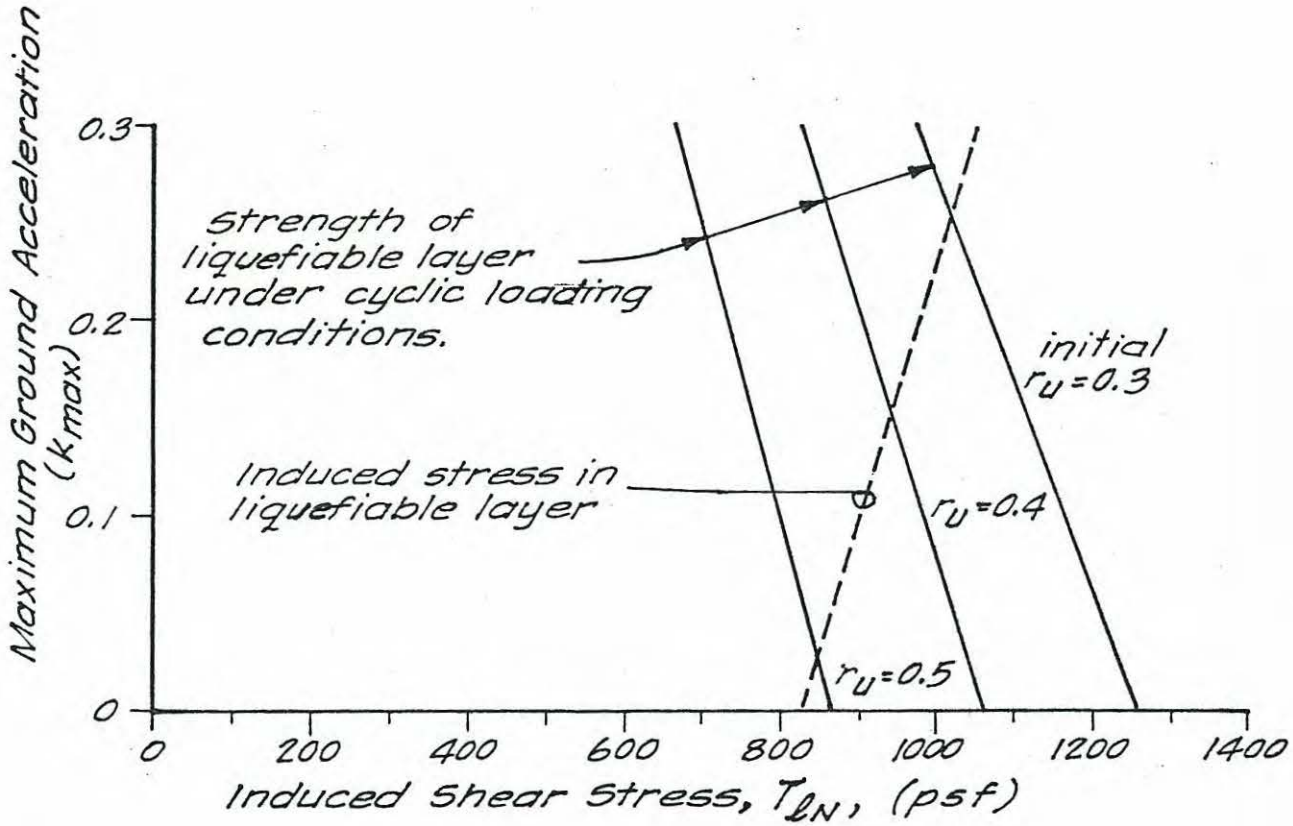

PARAMETERS:

Tails - $\gamma = 120$ psf

$H = 60$ ft.

Foundation Soils $\gamma = 125$ psf

$D_r = 75\%$

$\theta = 15°$

$$\tau_{lN} = \left(\frac{\sigma_{ds}}{2\sigma_a} f[k_{max}]\right)\sigma_o' \frac{\tau_{av}}{\tau_{max}} \frac{Dr}{50}$$

How is this obtained?

This is not the relationship presented in Seed & Idriss (1971)

See Seed & Idriss (1971) for Details of Analysis.

Project No. V77016 Drawn EG Reviewed SBF Date Dec/78

N

B.H. No 13 (T-6)
(El. 1880.59)

108000 E

B.H. No. 14 (T-7)
(El. 1790.93)

Approximate location of Excavated Tails

B.H. No 15
(El. 1607.16)

MON. No. 650.2

109000 E

B.H. No. 17
(052)

B.H.
(05

109,500 E

115,000

114,500

MON No 26

MON. No 264

MON. No. 650.1

MON. No. 500.1

1670
1660
1650
1640
1630
1620
1610
1600
1590

MON. No. 350.1

MON. No. 500.2

MON. No. 350.2

MON. No. 350.3

1700
1675
1650
1625
1600
1575
1550
1525
1500
1475
1450
1425
1400
1375
1350

114,000

1326

COMPOUND

MILL

B.H. No 12 (T-5)
(El. 1945.19)

B.H. No 16 (T-8)
(El. 1623.80)

MON No 24

MON No 24A

MON No 24B

MON. No. 24.0

TREE LINE

RECONTOURED TAILING RILE.

FIGURE 7

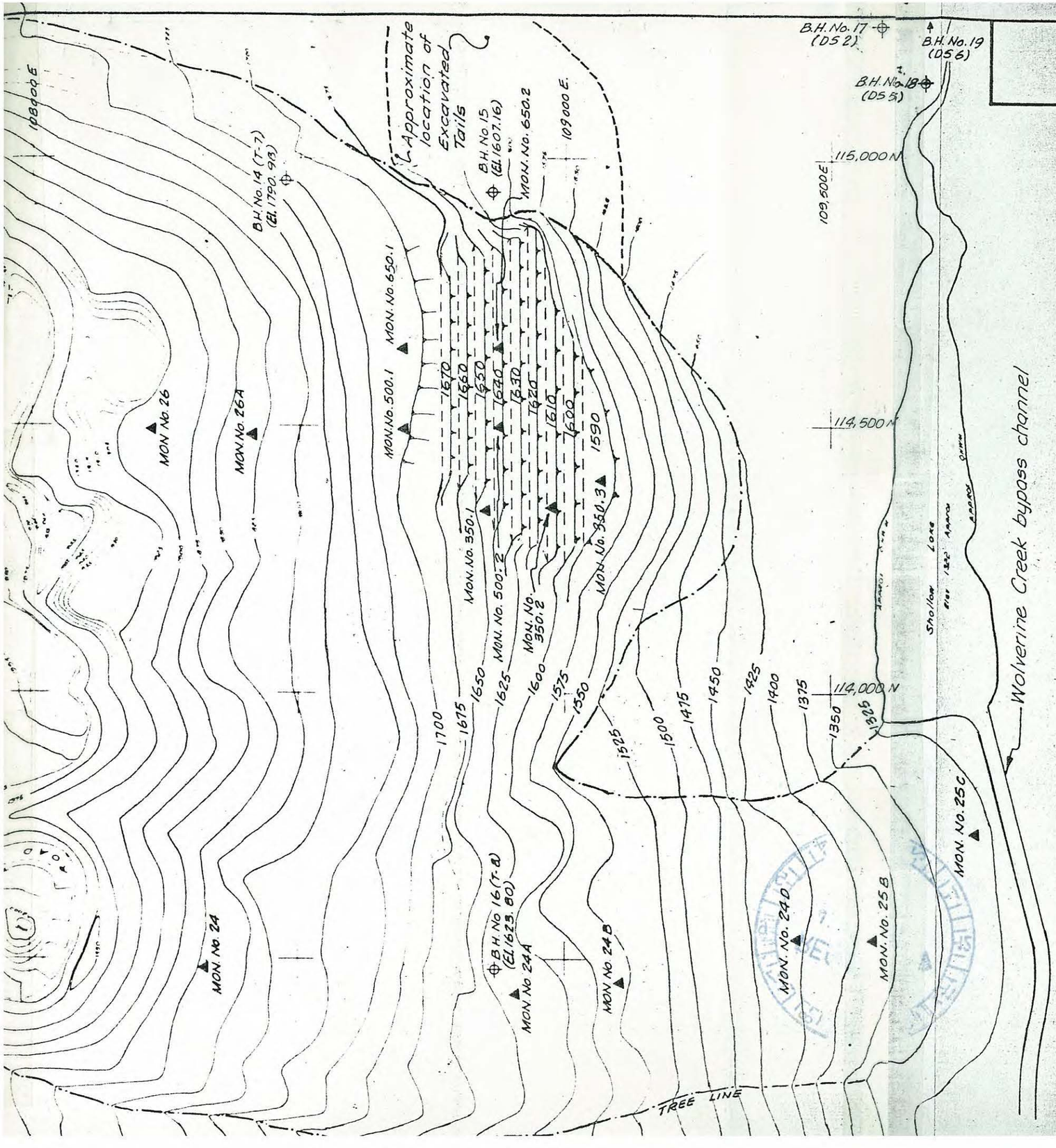

LEGEND:

MON. No. 19 ▲ Surface movement survey reference point.

B.H. No. 12 ⊕ Borehole

NOTE:

The contours shown on the 1974 failure lobe represent the average slopes of the recontoured area.

REFERENCE:

Topo. plan of Mill Tailings Pile for Clinton Creek Mine. by Underhill Engineering Ltd. - April 29, 1978. Coordinate grid from Cassiar Asbestos Corp. Grid Origin.

Scale: 1 in. to 200 ft.

Drawn lng
Reviewed
Date DEC. '78

Golder Associates

TC Library

JOURNAL OF THE GEOTECHNICAL ENGINEERING DIVISION

SIMPLIFIED PROCEDURE FOR ESTIMATING DAM AND EMBANKMENT EARTHQUAKE-INDUCED DEFORMATIONS

By Faiz I. Makdisi,[1] A. M. ASCE and H. Bolton Seed,[2] F. ASCE

INTRODUCTION

In the past decade major advances have been achieved in analyzing the stability of dams and embankments during earthquake loading. Newmark (13) and Seed (18) proposed methods of analysis for predicting the permanent displacements of dams subjected to earthquake shaking and suggested this as a criterion of performance as opposed to the concept of a factor of safety based on limit equilibrium principles. Seed and Martin (26) used the shear beam analysis to study the dynamic response of embankments to seismic loads and presented a rational method for the calculation of dynamic seismic coefficients for earth dams. Ambraseys and Sarma (1) adopted the same procedure to study the response of embankments to a variety of earthquake motions.

Later the finite element method was introduced to study the two-dimensional response of embankments (5,7) and the equivalent linear method (21) was used successfully to represent the strain-dependent nonlinear behavior of soils. In addition the nature of the behavior of soils during cyclic loading has been the subject of extensive research (10,20,23,29). Both the improvement in the analytical tools to study the response of embankments and the knowledge of material behavior during cyclic loading led to the development of a more rational approach to the study of stability of embankments during seismic loading. Such an approach was used successfully to analyze the Sheffield Dam failure during the 1925 Santa Barbara earthquake (24) and the behavior of the San Fernando Dams during the 1971 earthquake (25). This method has since been used extensively in the design and analysis of many large dams in the State of California and elsewhere.

Note.—Discussion open until December 1, 1978. To extend the closing date one month, a written request must be filed with the Editor of Technical Publications, ASCE. This paper is part of the copyrighted Journal of the Geotechnical Engineering Division, Proceedings of the American Society of Civil Engineers, Vol. 104, No. GT7, July, 1978. Manuscript was submitted for review for possible publication on August 30, 1977.

[1]Project Engr., Woodward-Clyde Consultants, San Francisco, Calif.
[2]Prof. of Civ. Engrg., Univ. of California, Berkeley, Calif

From the study of the performance of embankments during strong earthquakes, two distinct types of behavior may be discerned: (1) That associated with loose to medium dense sandy embankments, susceptible to rapid increases in pore pressure due to cyclic loading resulting in the development of pore pressures equal to the overburden pressure in large portions of the embankment, associated reductions in shear strength, and potentially large movements leading to almost complete failure; and (2) the behavior associated with compacted cohesive clays, dry sands, and some dense sands; here the potential for buildup of pore pressures is much less than that associated with loose to medium dense sands, the resulting cyclic strains are usually quite small, and the material retains most of its static undrained shearing resistance so that the resulting post-earthquake behavior is a limited permanent deformation of the embankment.

The dynamic analysis procedure proposed by Seed, et al. (25) has been used to predict adequately both types of embankment behavior using the "Strain Potential" concept. Procedures for integrating strain potentials to obtain the overall deformation of an embankment have been proposed by Seed, et al. (25), Lee (9), and Serff, et al. (27).

The dynamic analysis approach has been recommended by the Committee on Earthquakes of the International Commission on Large Dams (3): "high embankment dams whose failure may cause loss-of-life or major damage should be designed by the conventional method at first, followed by a dynamic analysis in order to investigate any deficiencies which may exist in the pseudo-statical design of the dam." For low dams in remote areas the Committee recommended the use of conventional pseudostatic methods using a constant horizontal seismic coefficient selected on the basis of the seismicity of the area. However, the inadequacy of the pseudostatic approach to predict the behavior of embankments during earthquakes has been clearly recognized and demonstrated (19,24,25,26, 28). Furthermore in the same report (3) the Commission refers to the conventional method as follows: "There is a need for early revision of the conventional method since the results of dynamic analyses, model tests and observations of existing dams show that the horizontal acceleration due to earthquake forces varies throughout the height of the dam . . . in several instances, this method predicts a safe condition for dams which are known to have had major slides."

It is this need for a simple yet rational approach to the seismic design of small embankments that prompted the development of the simplified procedure described herein.

This approximate method uses the concept originally proposed by Newmark (13) for calculating permanent deformations but it is based on an evaluation of the dynamic response of the embankment as proposed by Seed and Martin (26) rather than rigid body behavior. It assumes that failure occurs on a well-defined slip surface and that the material behaves elastically at stress levels below failure but develops a perfectly plastic behavior above yield. The method involves the following steps:

1. A yield acceleration, i.e., an acceleration at which a potential sliding surface would develop a factor of safety of unity is determined. Values of yield acceleration are a function of the embankment geometry, the undrained strength of the material (or the reduced strength due to shaking), and the location of the potential sliding mass.

2. Earthquake induced accelerations in the embankment are determined using dynamic response analyses. Finite element procedures using strain-dependent soil properties can be used for calculating time histories of acceleration, or simpler one-dimensional techniques might be used for the same purpose. From these analyses, time histories of average accelerations for various potential sliding masses can be determined.

3. For a given potential sliding mass, when the induced acceleration exceeds the calculated yield acceleration, movements are assumed to occur along the direction of the failure plane and the magnitude of the displacement is evaluated by a simple double integration procedure.

The method has been applied to dams with heights in the range of 100 ft–200 ft (30 m–60 m), and constructed of compacted cohesive soils or very dense cohesionless soils, but may be applicable to higher embankments. A similar approach has been proposed by Sarma (16) using the assumption of a rigid block on an inclined plane rather than a deformable earth structure that responds with differential motions to the imposed base excitation.

In the following sections the steps involved in the analyses will be described in detail and design curves prepared on the basis of analyzed cases will be presented, together with an example problem to illustrate the use of the method. Note, however, that the method is an approximate one and involves simplifying assumptions. The design curves are averages based on a limited number of cases analyzed and should be updated as more data become available and more cases are studied.

Determination of Yield Acceleration

The yield acceleration, k_y, is defined as that average acceleration producing a horizontal inertia force on a potential sliding mass so as to produce a factor of safety of unity and thus cause it to experience permanent displacements.

For soils that do not develop large cyclic strains or pore pressures and maintain most of their original strength after earthquake shaking, the value of k_y can be calculated by stability analyses using limiting equilibrium methods. In conventional slope stability analyses the strength of the material is defined as either the maximum deviator stress in an undrained test, or the stress level that would cause a certain allowable axial strain, say 10%, in a test specimen. However, the behavior of the material under cyclic loading conditions is different than that under static conditions. Due to the transient nature of the earthquake loading, an embankment may be subjected to a number of stress pulses at levels equal to or higher than its static failure stress that simply produce some permanent deformation rather than complete failure. Thus the yield strength is defined, for the purpose of this analysis, as that maximum stress level below which the material exhibits a near elastic behavior (when subjected to cyclic stresses of numbers and frequencies similar to those induced by earthquake shaking) and above which the material exhibits permanent plastic deformation of magnitudes dependent on the number and frequency of the pulses applied. Fig. 1 shows the concept of cyclic yield strength. The material in this case has a cyclic yield strength equal to about 90% of its static undrained strength and as shown in Fig. 1(*a*) the application of 100 cycles of stress amounting to 80%

of the undrained strength resulted in essentially an elastic behavior with very little permanent deformation. On the other hand, the application of 10 cycles of stress level equal to 95% of the static undrained strength led to substantial permanent strain as shown in Fig. 1(*b*). On loading the material monotonically to failure after the series of cyclic stress applications, the material was found to retain the original undrained strength. This type of behavior is associated with various types of soils that exhibit small increases in pore pressure during cyclic loading. This would include clayey materials, dry or partially saturated cohesionless soils, or very dense saturated cohesionless materials that will not undergo significant deformations, even under cyclic loading conditions, unless the undrained static strength of the soil is exceeded.

Seed and Chan (20) conducted cyclic tests on samples of undisturbed and compacted silty clays and found that for conditions of no stress reversal and for different values of initial and cyclic stresses, the total stress required to produce large deformations in 10 cycles and 100 cycles ranged between 90%–110% of the undrained static strength.

Sangrey, et al. (15) investigated the effective stress response of clay under repeated loading. They tested undisturbed samples of clay (LL = 28, PI = 10) and found that the cyclic yield strength of this material was of the order of 60% of its static undrained strength.

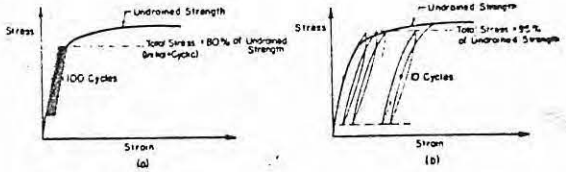

FIG. 1.—Determination of Dynamic Yield Strength

Rahman (14) performed similar tests on remolded samples of a brittle silty clay (LL = 91, PI = 49) and found that the cyclic yield strength was a function of the initial effective confining pressure. For practical ranges of effective confining pressures the cyclic yield strength for this material ranged between 80%–95% of its static undrained strength. At cyclic stress levels below the yield strength, in all cases, the material reached equilibrium and assumed an elastic behavior at strain levels less than 2% irrespective of the number of stress cycles applied.

Thiers and Seed (28) performed tests on undisturbed and remolded samples of different clayey materials to determine the reduction in static undrained strength due to cyclic loading. Their results are summarized in Fig. 2 which shows the reduction in undrained strength after cyclic loading as a function of the ratio of the "maximum cyclic strain" to the "static failure strain." These results were obtained from strain controlled cyclic tests; after the application of 200 cycles of a certain strain amplitude, the sample was loaded to failure monotonically at a strain rate of 3%/min. Thus from Fig. 2 it could be argued that if a clay is subjected to 200 cycles of strain with an amplitude less than half its static failure strain, the material may be expected to retain at least 90% of its original static undrained strength.

Andersen (2), on the basis of cyclic simple shear tests on samples of Drammen clay, determined that the reduction in undrained shear strength was found to be less than 25% as long as the cyclic shear strain was less than ±3% even after 1,000 cycles. Some North Sea clays, however, have shown a strength reduction of up to 40% for the same level of cyclic loading.

On the basis of the experimental data reported previously and for values of cyclic shear strains calculated from earthquake response analyses, the value of cyclic yield strength for a clayey material can be estimated. In most cases this value would appear to be 80% or more of the static undrained strength. This value in turn may be used in an appropriate method of stability analysis to calculate the corresponding yield acceleration.

Finite element response analyses (as will be described later) have been carried out to calculate time histories of crest acceleration and average acceleration

TABLE 1.—Maximum Cyclic Shear Strains Calculated from Dynamic Finite Element Response Analyses

Magnitude (1)	Embankment height, in feet (2)	Slope, *H*:*V* (3)	Maximum base acceleration, *g* (4)	Maximum shear strain, as a percentage (5)
6-1/2 (Caltech record)	75	2:1	0.5	0.2–0.4
6-1/2 (Caltech record)	150	2:1	0.2	0.1–0.15
6-1/2 (Caltech record)	150	2:1	0.5	0.2–0.3
6-1/2 (Lake Hughes record)	150	2:1	0.2	0.1–0.15
6-1/2 (Caltech record)	150	2-1/2:1	0.5	0.2–0.3
7-1/2 (Taft record)	150	2:1	0.5	0.2–0.5
7-1/2 (Taft record)	150	2:1	0.2	0.1–0.2
8-1/4 (S-I record)	150	2:1	0.75	0.4–1.0
8-1/4 (S-I record)	135	—	0.4	0.2–0.5

Note: 1 ft = 0.305 m.

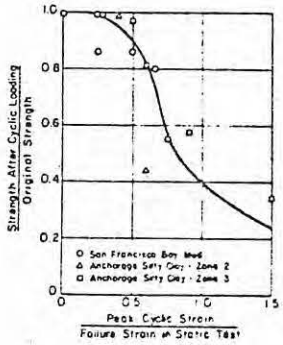

FIG. 2.—Reduction in Static Undrained Strength Due to Cyclic Loading (29)

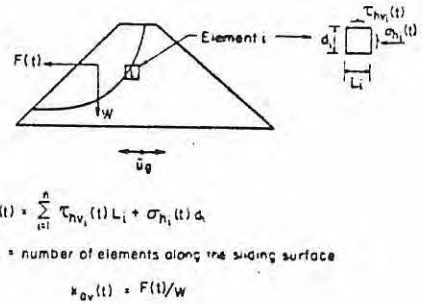

FIG. 3.—Calculation of Average Acceleration from Finite Element Response Analysis

for various potential sliding masses. The method of analysis employs the equivalent linear technique with strain-dependent modulus and damping. The ranges of calculated maximum shear strains, for different magnitude earthquakes and different embankment characteristics, are presented in Table 1. It can be seen from Table 1 that the maximum cyclic shear strain induced during the earthquakes ranged between 0.1% for a magnitude 6-1/2 earthquake with a base acceleration of 0.2 g and 1% for a magnitude 8-1/4 earthquake with a base acceleration of 0.75 g. For the compacted clayey material encountered in dam embankments "static failure strain" values usually range between 3%–10%, depending on whether the material was compacted on the dry or wet side of the optimum moisture content. Thus in both instances the ratio of the "cyclic strain" to "static failure strain" is less than 0.5.

It seems reasonable, therefore, to assume that for these compacted cohesive soils, very little reduction in strength may be expected as a result of strong earthquake loading of the magnitude described previously.

Once the cyclic yield strength is defined, the calculation of the yield acceleration can be achieved by using one of the available methods of stability analysis. In the present study the ordinary method of slices has been used to calculate the yield acceleration for circular slip surfaces using a pseudostatic analysis. As an alternative one of the writers (18) has suggested a method of combining both effective and total stress approaches, where the shear strength on the failure plane during the earthquake is considered to be a function of the initial effective normal stress on that same plane before the earthquake. This method is applicable to noncircular slip surfaces and the horizontal inertia force resulting in a factor of safety of unity can readily be calculated.

Having determined the yield acceleration for a certain location of the slip surface, the next step in the analysis is to determine the time history of earthquake-induced average accelerations for that particular sliding mass. This will be treated in the following section.

Determination of Earthquake Induced Acceleration

In order for the permanent deformations to be calculated for a particular slip surface, the time history of earthquake induced average accelerations must first be determined.

Two-dimensional finite element procedures using equivalent linear strain-dependent properties are available (6) and have been shown to provide response values in good agreement with measured values (8) and with closed-form one-dimensional wave propagation solutions (17).

For most of the case studies of embankments used in the present analysis the response calculation was performed using the finite element computer program QUAD-4 (6) with strain-dependent modulus and damping. The program uses the Rayleigh damping approach and allows for variable damping to be used in different elements.

To calculate the time history of average acceleration for a specified sliding mass, the method described by Chopra (4) was adopted in the present study. The finite element calculation provides time histories of stresses for every element in the embankment. As shown in Fig. 3, at each time step the forces acting along the boundary of the sliding mass are calculated from the corresponding

normal and shear stresses of the finite elements along that boundary. The resultant of these forces divided by the weight of the sliding mass would give the average acceleration, $k_{av}(t)$, acting on the sliding mass at that instant in time. The process is repeated for every time step to calculate the entire time history of average acceleration.

For a 150-ft (46-m) high dam subjected to 30 sec of the Taft earthquake record scaled to produce a maximum base acceleration of 0.2 g, the variation

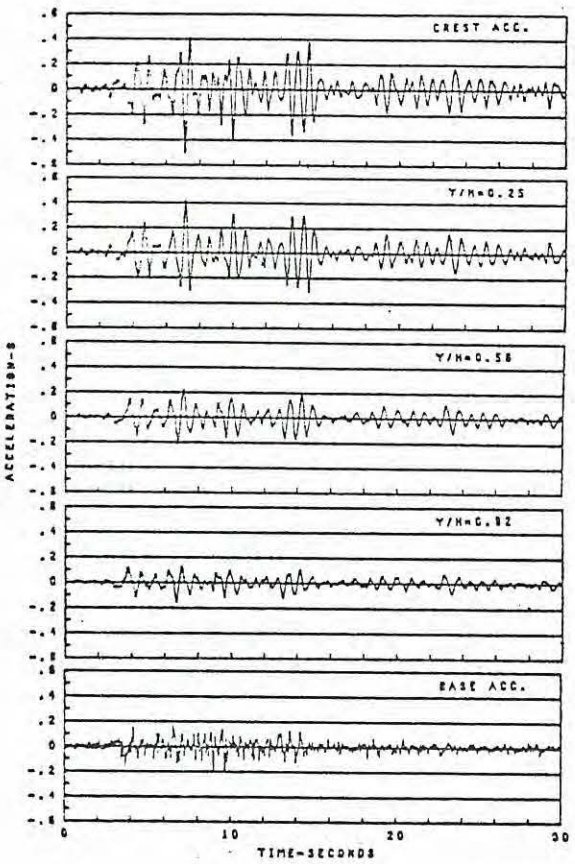

FIG. 4.—Time Histories of Average Acceleration for Various Depths of Potential Sliding Mass

of the time history of k_{av} with the depth of the sliding mass within the embankment, together with the time history of crest accelerations, is shown in Fig. 4.

Comparing the time history of crest acceleration with that of the average acceleration for different depths of the potential sliding mass, the similarity in the frequency content is readily apparent (it generally reflects the first natural period of the embankment), while the amplitudes are shown to decrease as the depth of the sliding mass increases towards the base of the embankment. The maximum crest acceleration is designated by $\ddot{u}_{max}$, and k_{max} is the maximum

average acceleration for a potential sliding mass extending to a specified depth, y.

It would be desirable to establish a relationship showing the variation of the maximum acceleration ratio, $k_{max}/\ddot{u}_{max}$, with depth for a range of embankments and earthquake loading conditions. It would then be sufficient, for design purposes, to estimate the maximum crest acceleration in a given embankment due to a specified earthquake and use this relationship to determine the maximum average acceleration for any depth of the potential sliding mass. A simplified procedure to estimate the maximum crest acceleration and the natural period

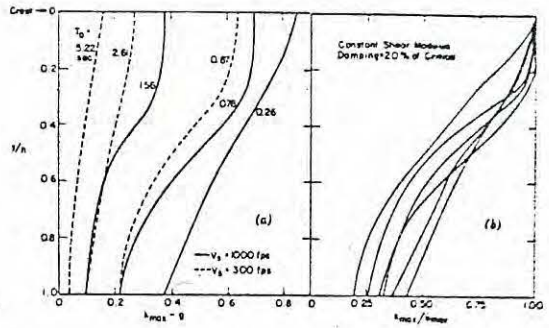

FIG. 5.—El Centro Record (12): (*a*) Variation of Maximum Average Acceleration with Depth of Sliding; (*b*) Variation of Ratio of Average Acceleration to Maximum Crest Acceleration with Depth of Sliding Surface

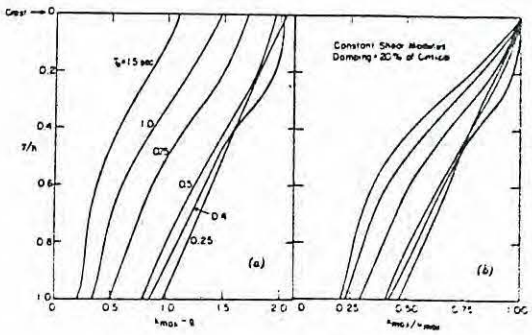

FIG. 6.—Average of Eight Strong Motion Records (1): (*a*) Variation of Maximum Average Acceleration with Depth of Sliding Mass; (*b*) Variation of Ratio of Maximum Average Acceleration to Maximum Crest Acceleration with Depth of Sliding Surface

of an embankment subjected to a given base motion is described in Appendix A of Ref. 11.

To determine the variation of maximum acceleration ratio with depth, use was made of published results of response computations using the one-dimensional shear slice method with visco-elastic material properties (1,26). Martin (12) calculated the response of embankments ranging in height between 100 ft–600 ft (30 m–180 m) and with shear wave velocities between 300 fps–1,000 fps (92 m/s–300 m/s). Using a constant shear modulus and a damping factor of 0.2,

the average acceleration histories for various levels were computed for embankments subjected to ground accelerations recorded in the El Centro earthquake of 1940. The variation of the maximum average acceleration, k_{max}, with depth for these embankments with natural periods ranging between 0.26 sec–5.22 sec is presented in Fig. 5(*a*). The maximum average acceleration in Fig. 5(*a*) is normalized with respect to the maximum crest acceleration and the ratio, $k_{max}/\ddot{u}_{max}$, plotted as a function of the depth of the sliding mass is presented in Fig. 5(*b*).

Ambraseys and Sarma (1) used essentially the same method reported by Seed and Martin (26) and calculated the response of embankments with natural periods ranging between 0.25 sec and 3.0 sec. They presented their results in terms of average response for eight strong motion records. The variation of maximum average acceleration with depth based on the results reported by Ambraseys and Sarma (1) is shown in Fig. 6(*a*) and that for the maximum acceleration ratio, $k_{max}/\ddot{u}_{max}$, is shown in Fig. 6(*b*). A summary of the results obtained

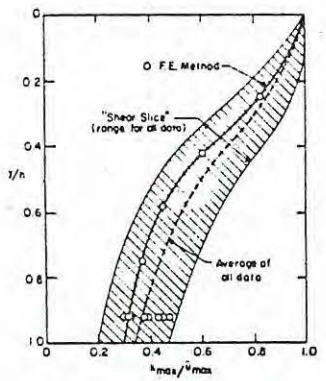

FIG. 7.—Variation of Maximum Acceleration Ratio with Depth of Sliding Mass

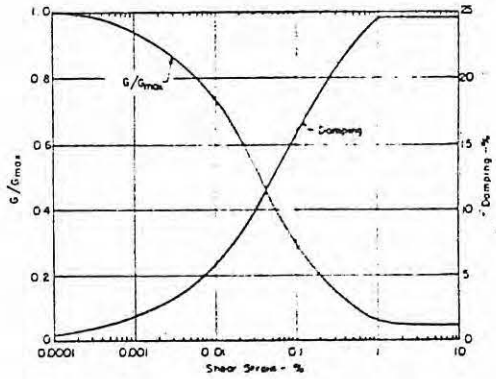

FIG. 8.—Shear Modulus and Damping Characteristics Used in Response Computations

from the different shear slice response calculations mentioned previously is presented in Fig. 7 together with results obtained from finite element calculations made in the present study. As can be seen from Fig. 7 the shape of the curves obtained using the shear slice method and the finite element method are very similar. The dashed curve in Fig. 7 is an average relationship of all data considered. The maximum difference between the envelope of all data and the average relationship ranges from ±10% to ±20% for the upper portion of the embankment and from ±20% to ±30% for the lower portion of the embankment.

Considering the approximate nature of the proposed method of analysis, the use of the average relationship shown in Fig. 7 for determining the maximum average acceleration for a potential sliding mass based on the maximum crest acceleration is considered accurate enough for practical purposes. For design computations where a conservative estimate of the accelerations is desired the upper bound curve shown in Fig. 7 may be used leading to values that are 10%–30% higher than those estimated using the average relationship.

CALCULATION OF PERMANENT DEFORMATIONS

Once the yield acceleration and the time history of average induced acceleration for a potential sliding mass have been determined, the permanent displacements can readily be calculated.

By assuming a direction of the sliding plane and writing the equation of motion for the sliding mass along such a plane, the displacements that would occur any time the induced acceleration exceeds the yield acceleration may be evaluated by simple numerical integration. For the purposes of the soil types considered in this study, the yield acceleration was assumed to be constant throughout the earthquake.

The direction of motion for a potential sliding mass once yielding occurs

TABLE 2.—Embankment Characteristics for Magnitude 6-1/2 Earthquake

Case number (1)	Embankment description (2)	Height, in feet (3)	Base acceleration, g (4)	T_0, in seconds (5)[a]	k_{max}, g (6)[b]	Symbol[c] (7)
1	Example slope = 2:1 k_{2max} = 60	150	0.2 (Caltech record)	0.8	(1) 0.31 (2) 0.12	● ■
2	Example slope = 2:1 k_{2max} = 60	150	0.5 (Caltech record)	1.08	(1) 0.4 (2) 0.18	○ □
3	Example slope = 2:1 k_{2max} = 80	150	0.5 (Lake Hughes record)	0.84	(1) 0.33 (2) 0.16	⊙ △
4	Example slope = 2-1/2:1 k_{2max} = 80	150	0.5 (Caltech record)	0.95	(1) 0.49 (2) 0.22	◇ ▽
5	Example slope = 2:1 k_{2max} = 60	75	0.5 (Caltech record)	0.6	(1) 0.86 (2) 0.26	◑ ◪

[a] Calculated first natural period of the embankment.

[b] Maximum value of time history of: (1) Crest acceleration; and (2) average acceleration for sliding mass extending through full height of embankment.

[c] Legend used in Fig. 9(*a*).

Note: 1 ft = 0.305 m.

was assumed to be along a horizontal plane. This mode of deformation is not uncommon for embankments subjected to strong earthquake shaking, and is manifested in many cases in the field by the development of longitudinal cracks along the crest of the embankment. However studies made for other directions of the sliding surface showed that this factor had little effect on the computed displacements (11).

To calculate an order of magnitude of the deformations induced in embankments due to strong shaking a number of cases have been analyzed during the course of this study. The height of embankments considered ranged between 75 ft–150 ft (23 m–46 m) with varying slopes and material properties. The embankments were subjected to ground accelerations representing three different earthquake magnitudes: 6-1/2, 7-1/2, and 8-1/4.

The method used for calculating the response, as mentioned earlier, is a time-step finite element analysis using the equivalent linear method. The strain-dependent modulus and damping relations for the soils used in this study are

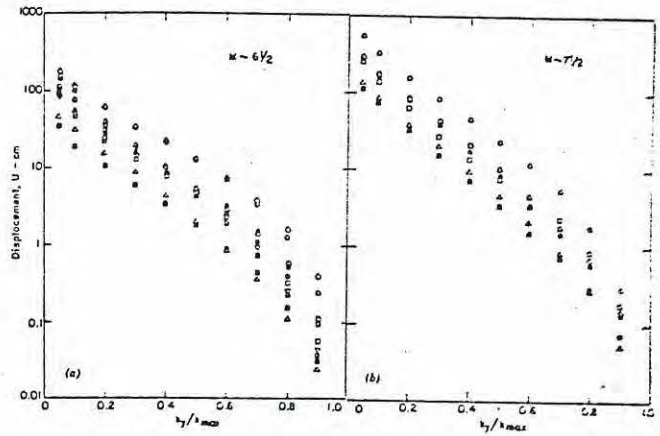

FIG. 9.—Variation of Permanent Displacement with Yield Acceleration: (*a*) Magnitude 6-1/2 Earthquake; (*b*) Magnitude 7-1/2 Earthquake

presented in Fig. 8. The response computation for each base motion was repeated for a number of iterations (mostly 3–4) until strain compatible material properties were obtained. In each case both time histories of crest acceleration and the average acceleration for a potential sliding mass extending through almost the full height of the embankment were calculated, together with the first natural period of the embankment. In one case however, time histories of average acceleration for sliding surfaces at five different levels in the embankment were obtained (see Fig. 4), and the corresponding permanent deformations for each time history were calculated for different values of yield acceleration. It was found that for the same ratio of yield acceleration to maximum average acceleration at each level, the computed deformations varied uniformly between a maximum value obtained using the crest acceleration time history to a minimum value obtained using the time history of average acceleration for a sliding mass extending through the full height of the embankment. Thus it was considered

sufficient for the remaining cases to compute the deformations only for these two levels.

Table 2 shows details of the embankments analyzed using ground motions representative of a magnitude 6-1/2 earthquake. The two rock motions used were those recorded at the Cal Tech Seismographic Laboratory (S90W Component) and at Lake Hughes Station No. 12 (N12E) during the 1971 San Fernando earthquake, with maximum accelerations scaled to 0.2 g and 0.5 g. The computed natural periods and maximum values of the acceleration time histories are also presented in Table 2. The computed natural periods ranged between a value of 0.6 sec for the 75-ft (23-m) high embankment to a value of 1.08 sec for the 150-ft (46-m) high embankment. Because of the nonlinear strain-dependent

TABLE 3.—Embankment Characteristics for Magnitude 7-1/2 Earthquake

Case number (1)	Embankment description (2)	Height, in feet (3)	Base acceleration, g (4)	T_0, in seconds (5)[a]	k_{max}, g (6)[b]	Symbol[c] (7)
1	Example slope = 2:1 k_{2max} = 60	150	0.2 (Taft record)	0.86	(1) 0.41 (2) 0.13	● ■
2	Example slope = 2:1 k_{2max} = 60	150	0.5 (Taft record)	1.18	(1) 0.54 (2) 0.21	○ □
3	Example slope = 2-1/2:1 k_{2max} = 80	150	0.2 (Taft record)	0.76	(1) 0.46 (2) 0.15	⊙ △

[a]Calculated first natural period of the embankment.
[b]Maximum value of time history of: (1) Crest acceleration; and (2) average acceleration for sliding mass extending through full height of embankment.
[c]Legend used in Fig. 9(*b*).
Note: 1 ft = 0.305 m.

behavior of the material, the response of the embankment is highly dependent on the amplitude of the base motion. This is clearly demonstrated in the first two cases in Table 2, where the same embankment was subjected to the same ground acceleration history but with different maximum accelerations for each case. In one instance, for a base acceleration of 0.2 g the calculated maximum crest accelerations was 0.3 g with a magnification of 1.5 and a computed natural period of the order of 0.8 sec. In the second case, for a base acceleration of 0.5 g the computed maximum crest acceleration was 0.4 g with an attenuation of 0.8 and a computed natural period of 1.1 sec.

From the time histories of induced acceleration calculated for all the cases

described in Table 2 and for various ratios of yield acceleration to maximum average acceleration, k_y/k_{max}, the permanent deformations were calculated by numerical double integration. The results are presented in Fig. 9(*a*) which shows that for relatively low values of yield acceleration, k_y/k_{max} of 0.2 for example, the range of computed permanent displacements was of the order of 10 cm–70 cm (4 in.–28 in.). However, for larger values of k_y/k_{max}, say 0.5 or more, the calculated displacements were less than 12 cm (4.8 in.). It should be emphasized that for very low values of yield accelerations (in this case $k_y/k_{max} \leq 0.1$) the basic assumptions used in calculating the response by the finite element

TABLE 4.—Embankment Characteristics of Magnitude 8-1/4 Earthquake

Case number (1)	Embankment description (2)	Height, in feet (3)	Base acceleration, g (4)	T_0, in seconds (5)[a]	k_{max}, g (6)[b]	Symbol[c] (7)
1	Chabot Dam (average properties)	135	0.4 (S-1 Synth. record)	0.99	(1) 0.57	○
	Chabot Dam (Lower bound)	135	0.4 (S-1 Synth. record)	1.07	(1) 0.53	△
	Chabot Dam (Upper bound)	135	0.4	0.83	(1) 0.68	□
2	Example slope = 2:1 k_{2max} = 60	150	0.75	1.49	(1) 0.74 (2) 0.34	● ■

[a]Calculated first natural period of the embankment.
[b]Maximum value of time history of: (1) Crest acceleration; and (2) average acceleration for sliding mass extending through full height of embankment.
[c]Legend used in Fig. 10(*a*).
Note: 1 ft = 0.305 m.

method, i.e., the equivalent linear behavior and the small strain theory, become invalid. Consequently, the acceleration time histories calculated for such a case do not represent the real field behavior and the calculated displacements based on these time histories may not be realistic.

The procedure described previously was repeated for the case of a magnitude 7-1/2 earthquake. The base acceleration time history used for this analysis was that recorded at Taft during the 1952 Kern County earthquake and scaled to maximum accelerations of 0.2 g and 0.5 g. The details of the three cases analyzed are presented in Table 3 and the results of the computations of the

permanent displacements are shown in Fig. 9(*b*). For a ratio of k_y/k_{max} of 0.2 the calculated displacements in this case ranged between 30 cm–200 cm (12 in.–80 in.), and for ratios greater than 0.5 the displacements were less than 25 cm (0.8 ft).

In the cases analyzed for the 8-1/4 magnitude earthquake, an artificial accelerogram proposed by Seed and Idriss (21) was used with maximum base accelerations of 0.4 *g* and 0.75 *g*. Two embankments were analyzed in this case and their calculated natural periods ranged between 0.8 sec and 1.5 sec. Table 4 shows the details of the calculations and in Fig. 10(*a*) the results of the permanent displacement computations are presented. As can be seen from Fig. 10(*a*) the permanent displacements computed for a ratio of k_y/k_{max} of 0.2 ranged between 200 cm–700 cm (80 in.–28 in.). and for ratios higher than 0.5 the values were less than 100 cm (40 in.). Note in this case that values of deformations calculated for a yield ratio less than 0.2 may not be realistic.

An envelope of the results obtained for each of the three earthquake loading

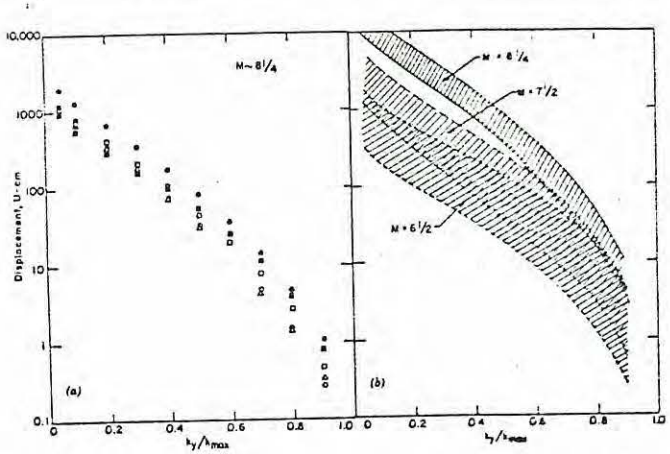

FIG. 10.—Variation of Permanent Displacement with Yield Acceleration: (*a*) Magnitude 8-1/4 Earthquake; (*b*) Summary of All Data

conditions is presented in Fig. 10(*b*) and reveals a large scatter in the computed results reaching, in the case of the magnitude 6-1/2 earthquake, about one order of magnitude.

It can reasonably be expected that for a potential sliding mass with a specified yield acceleration, the magnitude of the permanent deformation induced by a certain earthquake loading is controlled by the following factors: (1) The amplitude of induced average accelerations, which is a function of the base motion, the amplifying characteristics of the embankment, and the location of the sliding mass within the embankment; (2) the frequency content of the average acceleration time history, which is governed by the embankment height and stiffness characteristics, and is usually dominated by the first natural frequency of the embankment; and (3) the duration of significant shaking, which is a function of the magnitude of the specified earthquake.

Thus to reduce the large scatter exhibited in the data in Fig. 10(*b*), the permanent

displacements for each embankment were normalized with respect to its calculated first natural period, T_0, and with respect to the maximum value, k_{max}, of the average acceleration time history used in the computation. The resulting normalized permanent displacements for the three different earthquakes are presented in Fig. 11(*a*). It may be seen that a substantial reduction in the scatter of the data is achieved by this normalization procedure as evidenced by comparing the results in Figs. 10(*b*) and 11(*a*). This shows that for the ranges of embankment heights considered in this study [75 ft–150 ft (50 m–65 m)] the first natural period of the embankment and the maximum value of acceleration time history may be considered as two of the parameters having a major influence on the calculated permanent displacements. Average curves for the normalized permanent displacements based on the results in Fig. 11(*a*) are presented in Fig. 11(*b*). Although some scatter still exists in the results as shown in Fig. 11(*a*), the average curves presented in Fig. 11(*b*) are considered adequate to provide an order of magnitude of the induced permanent displacements for different

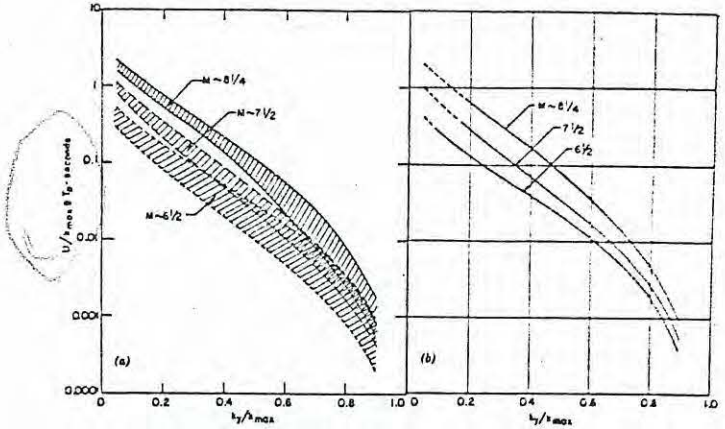

FIG. 11.—Variation of Yield Acceleration with: (*a*) Normalized Permanent Displacement—Summary of All Data; and (*b*) Average Normalized Displacement

magnitude earthquakes. At yield acceleration ratios less than 0.2 the average curves are shown as dashed lines since, as mentioned earlier, the calculated displacements at these low ratios may be unrealistic.

Thus, to calculate the permanent deformation in an embankment constructed of a soil that does not change in strength significantly during an earthquake, it is sufficient to determine its maximum crest acceleration, $\ddot{u}_{max}$, and first natural period, T_0, due to a specified earthquake. Then by the use of the relationship presented in Fig. 7, the maximum value of average acceleration history, k_{max}, for any level of the specified sliding mass may be determined. Entering the curves in Fig. 11(*b*) with the appropriate values of k_{max} and T_0, the permanent displacements can be determined for any value of yield acceleration associated with that particular sliding surface.

It has been assumed earlier in this paper that in the majority of embankments, permanent deformations usually occur due to slip of a sliding mass on a horizontal failure plane. For those few instances where sliding might occur on an inclined

failure plane it is of interest to determine the difference between the actual deformations and those calculated with the assumption of a horizontal failure plane having the same yield acceleration. A simple computation was made to investigate this condition using the analogy of a block on an inclined plane for a purely frictional material. It was found that for inclined failure planes with slope angles of 15° to the horizontal, the computed displacements were 10%–18% higher than those based on a horizontal plane assumption.

Application of Method to Embankment Subjected to 8-1/4 Magnitude Earthquake

To illustrate the use of the simplified procedure for evaluating earthquake-induced deformations, computations are presented herein for the 135-ft (41-m) high Chabot Dam, constructed of sandy clay and having the section shown in Fig. 12.

The shear wave velocity of the embankment was determined from a field investigation and the strain-dependent modulus and damping were determined from laboratory tests on undisturbed samples. The dam, located about 20 miles

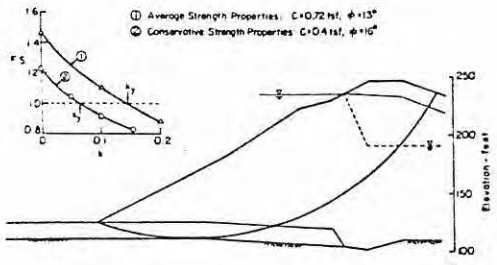

FIG. 12.—Yield Acceleration Values for Slide Mass Extending through Full Height of Embankment

(32 km) from the San Andreas fault, was shaken in 1906 by the magnitude 8-1/4 San Francisco earthquake with no significant deformations being noted; peak accelerations in the rock underlying the dam in this event are estimated to have been about 0.4 g. Accordingly the response of the embankment to ground accelerations representative of a magnitude 8-1/4 earthquake and having a maximum acceleration of 0.4 g was calculated by a finite element analysis. The maximum crest acceleration of the embankment, $\ddot{u}_{max}$, was calculated to be 0.57 g and the first natural period, $T_0 = 0.99$ sec. The maximum values of the calculated shear strain were less than 0.5%. On the basis of static undrained tests on the embankment material, the static failure strains ranged between 3%–8%, so that for the purposes of this analysis the cyclic yield strength of this material can be considered equal to its static undrained strength. From consolidated undrained tests on representative samples of the embankment material two interpretations were made for the strength of the material: (1) Based on an average of all the samples tested resulting in a cohesion value, c, of 0.72 tsf (69 kN/m^2) and a friction angle, ϕ, of 13°; and (2) a conservative interpretation, based on the minimum strength values with a cohesion of 0.4 tsf (38 kN/m^2) and a friction angle of 16°. Using these strength estimates, values of yield accelerations were calculated for a sliding mass extending through the full height of the embankment as shown in Fig. 12.

Considering the average relationship of $k_{max}/\ddot{u}_{max}$ with depth shown in Fig. 7, the ratio for a sliding mass extending through the full height of the embankment ($y/h = 0.95$) is 0.35, resulting in a maximum average acceleration, k_{max}, of $0.35 \times 0.57\ g = 0.2\ g$. From Fig. 12 the yield acceleration calculated for the average strength values is 0.14 g. Thus the parameters to be used in Fig. 11(b) to calculate the displacements for this particular sliding surface are as follows: magnitude = 8-1/4; $T_0 = 0.99$ sec; $k_{max} = 0.2$; and $k_y/k_{max} = 0.14/0.20 = 0.7$. From Fig. 11($b$): $U/k_{max}g\ T_0 = 0.013$ sec, therefore, the displacement $U = 0.013 \times 0.2 \times 32.2 \times 0.99 = 0.08$ ft (0.02 m).

Using the most conservative value of $k_{max}/\ddot{u}_{max}$ shown in Fig. 7 of 0.47, the computed displacement would have been 0.58 ft (0.18 m). Similarly using the conservative strength parameters for the soil (giving $k_y = 0.07$) and the average curve for $k_{max}/\ddot{u}_{max}$ shown in Fig. 7, the computed displacement would have been 1.5 ft (0.45 m). All of these values are in reasonable accord with the observed performance of the dam during the 1906 earthquake.

The calculation was repeated for a sliding mass extending through half the depth of the embankment. The computed permanent displacements ranged between 0.02 ft–1.08 ft (0.006 m–0.33 m) indicating that the critical potential sliding mass in this case was that extending through the full height of the embankment.

Conclusions

A simple yet rational approach to the design of small embankments under earthquake loading has been described herein. The method is based on the concept of permanent deformations as proposed by Newmark (13) but modified to allow for the dynamic response of the embankment as proposed by Seed and Martin (26) and restricted in application to compacted clayey embankments and dry or dense cohesionless soils that experience very little reduction in strength due to cyclic loading. The method is an approximate one and involves a number of simplifying assumptions that may lead to somewhat conservative results.

On the basis of response computations for embankments subjected to different ground motion records, a relationship for the variation of induced average acceleration with embankment depth has been established. Design curves to estimate the permanent deformations for embankments, in the height range of 100 ft–200 ft (30 m–60 m), have been established based on equivalent linear finite element dynamic analyses for different magnitude earthquakes. The use of these curves requires a knowledge of the maximum crest acceleration and the natural period of an embankment due to a specified ground motion.

It should be noted that the design curves presented are based on averages of a range of results that exhibit some degree of scatter, and are derived from a limited number of cases. These curves should be updated and refined as analytical results for more embankments are obtained.

Finally, the method has been applied to an actual embankment that was subjected to a magnitude 8-1/4 earthquake at an epicentral distance of some 20 miles. Depending on the degree of conservatism in estimating the undrained

strength of the material and in estimating the maximum accelerations in the embankment, the calculated deformations for this 135-ft (40-m) clayey embankment ranged between 0.1 ft–1.5 ft (0.3 m–0.46 m). These approximate displacement values are in good accord with the actual performance of the embankment during the earthquake.

Whereas the method described herein provides a rational approach to the design of embankments and offers a significant improvement over the conventional pseudostatic approach, the nature of the approximations involved requires that it be used with caution and good judgment especially in determining the soil characteristics of the embankment to which it may be applied.

For large embankments, for embankments where failure might result in a loss of life or major damage and property loss, or where soil conditions cannot be determined with a significant degree of accuracy to warrant the use of the method, the more rigorous dynamic method of analysis described earlier might well provide a more satisfactory alternative for design purposes.

Acknowledgment

The study described in this paper was conducted under the sponsorship of the National Science Foundation (Grant ENV 75-21875). The support of the National Science Foundation is gratefully acknowledged.

Appendix.—References

1. Ambraseys, N. N., and Sarma, S. K., "The Response of Earth Dams to Strong Earthquakes," *Geotechnique*, London, England, Vol. 17, Sept., 1967, pp. 181–213.
2. Andersen, K. H., "Behavior of Clay Subjected to Undrained Cyclic Loading," *Proceedings*, Conference on Behavior of Off-Shore Structures," Trondheim, Norway, Vol. 1, 1976, pp. 392–403.
3. "A Review of Earthquake Resistant Design of Dams," *Bulletin 27*, International Commission on Large Dams, Mar., 1975.
4. Chopra, A. K., "Earthquake Effects on Dams," thesis presented to the University of California, at Berkeley, Calif., in 1966, in partial fulfillment of the requirements for the degree of Doctor of Philosophy.
5. Clough, R. W., and Chopra, A. K., "Earthquake Stress Analysis in Earth Dams," *Journal of the Engineering Mechanics Division*, ASCE, Vol. 92, No. EM2, Proc. Paper 4793, Apr., 1966, pp. 197–212.
6. Idriss, I. M., et al., "QUAD-4, A Computer Program for Evaluating the Seismic Response of Soil Structures by Variable Damping Finite Elements," *Report No. EERC 73 16*, Earthquake Engineering Research Center, University of California, Berkeley, Calif., June, 1973.
7. Idriss, I. M., and Seed, H. B., "Response of Earth Banks During Earthquakes," *Journal of the Soil Mechanics and Foundations Division*, ASCE, Vol. 93, No. SM3, Proc. Paper 5232, May, 1967, pp. 61–82.
8. Kovacs, W. D., Seed, H. B., and Idriss, I. M., "Studies of Seismic Response of Clay Banks," *Journal of the Soil Mechanics and Foundations Division*, ASCE, Vol. 97, No. SM2, Proc. Paper 7878, Feb., 1971, pp. 441–455.
9. Lee, K. L., "Seismic Permanent Deformations in Earth Dams," *Report No. UCLA-ENG-7497*, School of Engineering and Applied Science, University of California at Los Angeles, Los Angeles, Calif., Dec., 1974.
10. Lee, K. L., and Seed, H. B., "Dynamic Strength of Anisotropically Consolidated Sand," *Journal of the Soil Mechanics and Foundations Division*, ASCE, Vol. 93, No. SM5, Proc. Paper 5451, Sept., 1967, pp. 169–190.
11. Makdisi, F. I., and Seed, H. B., "A Simplified Procedure for Computing Maximum Crest Acceleration and Natural Period for Embankments," *Report No. UCB/EERC-77/19*, Earthquake Engineering Research Center, University of California, Berkeley, Calif., 1977.
12. Martin, G. R., "The Response of Earth Dams to Earthquakes," thesis presented to the University of California, at Berkeley, Calif., in 1965, in partial fulfillment of the requirements for the degree of Doctor of Philosophy.
13. Newmark, N. M., "Effects of Earthquakes on Dams and Embankments," *Geotechnique*, London, England, Vol. 5, No. 2, June, 1965.
14. Rahman, M. S., "Undrained Behavior of Saturated Normally Consolidated Clay Under Repeated Loading," thesis presented to the Indian Institute of Technology, at Kharahpur, India, in July, 1972, in partial fulfillment of the requirements for the degree of Master of Science.
15. Sangrey, D., Henkel, D., and Esrig, M., "The Effective Stress Response of a Saturated Clay Soil to Repeated Loading," *Canadian Geotechnical Journal*, Vol. 6, No. 3, Aug., 1969, pp. 241–252.
16. Sarma, S. K., "Seismic Stability of Earth Dams and Embankments," *Geotechnique*, London, England, Vol. 25, No. 4, Dec., 1975, pp. 743–761.
17. Schnabel, P. B., and Seed, H. B., "Accelerations in Rock for Earthquakes in the Western United States," *Report No. EERC 72-2*, Earthquake Engineering Research Center, University of California, Berkeley, Calif., July, 1972.
18. Seed, H. B., "A Method for Earthquake-Resistant Design of Earth Dams," *Journal of the Soil Mechanics and Foundations Division*, ASCE, Vol. 92, No. SM1, Proc. Paper 4616, Jan., 1966, pp. 13–41.
19. Seed, H. B., "A Case Study of Seismic Instability and Terzaghi Foresight," Terzaghi Memorial Lecture Program, Bogazici University, Istanbul, Turkey, Aug. 14–16, 1973.
20. Seed, H. B., and Chan, C. K., "Clay Strength Under Earthquake Loading Conditions," *Journal of the Soil Mechanics and Foundations Division*, ASCE, Vol. 92, No. SM2, Proc. Paper 4723, Mar., 1966, pp. 53–78.
21. Seed, H. B., and Idriss, I. M., "Rock Motion Accelerograms for High Magnitude Earthquakes," *Report No. EERC 67-7*, Earthquake Engineering Research Center, University of California, Berkeley, Calif., Apr., 1969.
22. Seed, H. B., and Idriss, I. M., "Influence of Soil Conditions on Ground Motions During Earthquakes," *Journal of the Soil Mechanics and Foundations Division*, ASCE, Vol. 95, No. SM1, Proc. Paper 6347, Jan., 1969, pp. 99–137.
23. Seed, H. B., and Lee, K. L., "Liquefaction of Saturated Sands During Cyclic Loading," *Journal of the Soil Mechanics and Foundations Division*, ASCE, Vol. 92, No. SM6, Proc. Paper 4972, Nov., 1966, pp. 105–134.
24. Seed, H. B., Lee, K. L., and Idriss, I. M., "Analysis of the Sheffield Dam Failure," *Journal of the Soil Mechanics and Foundations Division*, ASCE, Vol. 95, No. SM6, Proc. Paper 6906, Nov., 1969, pp. 1453–1490.
25. Seed, H. B., et al., "Analysis of the Slides in the San Fernando Dams during the Earthquake of February 9, 1971," *Report No. EERC 73-2*, Earthquake Engineering Research Center, University of California, Berkeley, Calif., June, 1973.
26. Seed, H. B., and Martin, G. R., "The Seismic Coefficient in Earth Dam Design," *Journal of the Soil Mechanics and Foundations Division*, ASCE, Vol. 92, No. SM3, Proc. Paper 4824, May, 1966, pp. 25–58.
27. Serff, N., et al., "Earthquake Induced Deformations of Earth Dams," *Report No. EERC 76-4*, Earthquake Engineering Research Center, University of California, Berkeley, Calif., Sept., 1976.
28. Terzaghi, K., "Mechanisms of Landslides," The Geological Society of America, Engineering Geology (Berkey) Volume, Nov., 1950.
29. Thiers, G. R., and Seed, H. B., "Strength and Stress-Strain Characteristics of Clays Subjected to Seismic Loads," *ASTM STP 450*, Symposium on Vibration Effects of Earthquakes on Soils and Foundations, American Society for Testing and Materials, 1969, pp. 3–56.

3. Lamb, H., "On Waves due to a Travelling Disturbance," *Proceedings of the London Mathematical Society*, Vol. 35, 1903, pp. 141-148.
4. Lamb, H., "On the Propagation of Tremors over the Surface of an Elastic Solid," *Philosophical Transactions of the Royal Society of London*, Series A, Vol. 203, 1904, pp. 1-42.
5. Lamb, H., "On the Vibrations of an Elastic Plane Curved at One Point Whether Clamped or Simply Supported," *Proceedings of the London Mathematical Society*, Vol. 29, 1898, pp. 142-160.
6. Lysmer, J., "Vertical Motion of Rigid Footings," thesis presented to the University of Michigan, at Ann Arbor, Mich., in 1965, in partial fulfillment of the requirements for the degree of Doctor of Philosophy.
7. Lysmer, J., and Richart, F. E., Jr., "Dynamic Response of Footings to Vertical Loading," *Journal of the Soil Mechanics and Foundations Division*, ASCE, Vol. 92, No. SM1, Proc. Paper 4702, January, 1966, pp. 65-91.
8. Miller, G. F., and Pursey, H., "On the Partition of Energy between Elastic Waves in a Semi-Infinite Solid," *Proceedings of the Royal Society of London*, Series A, Vol. 233, 1955, pp. 55-69.
9. Quinlan, P. M., "The Elastic Theory of Soil Dynamics," *Symposium on the Dynamic Testing of Soils*, ASTM Special Publication No. 156, 1953, pp. 3-34.
10. Reissner, E., "Stationäre, axialsymmetrische durch eine schüttelnde Masse erregte Schwingungen eines homogenen elastischen Halbraumes," *Ingenieur-Archiv*, Vol. 7, Part 6, Dec., 1936, pp. 381-396.
11. Richart, F. E., Jr., Hall, J. R., Jr., and Woods, R. D., *Vibrations of Soils and Foundations*, Prentice-Hall, Inc., Englewood Cliffs, N.J., 1970, pp. 388-401; see also discussion in Chapter 7, pp. 191-213.
12. Roberts, J. A., "Forced Vertical Vibration of a Rigid Circular Disc on a Semi-Infinite Elastic Solid," *Proceedings of the Cambridge Philosophical Society*, Vol. 62, 1966, pp. 547-553.
13. Shah, P. M., "On the Dynamic Response of Foundation Systems," thesis presented to Rice University, at Houston, Tex., in 1968, in partial fulfillment of the requirements for the degree of Doctor of Philosophy.
14. Wei, Y. T., "Steady State Response of Certain Foundation Systems," thesis presented to Rice University, at Houston, Tex., in 1971, in partial fulfillment of the requirements for the degree of Doctor of Philosophy.

APPENDIX II.—NOTATION

The following symbols are used in this paper:

a_0 = dimensionless frequency parameter, defined by Eq. 6;
c_1, c_2 = dimensionless damping coefficients in Eq. 12;
c_{11}, c_{22}, c_{21} = dimensionless damping coefficients in Eqs. 10 and 11;
c_x, c_y = damping coefficients of dampers for model in Fig. 9;
$f_{11}, f_{22}, f_{12}, f_{21}$ = dimensionless flexibility coefficients in Eq. 3;
$g_{11}, g_{22}, g_{12}, g_{21}$ = dimensionless flexibility coefficients in Eq. 3;
$i = \sqrt{-1}$;
K_x = static lateral stiffness of disk, defined by P/u_{st} in Eq. 4;
K_ϕ = static rotational stiffness of disk, defined by M/ϕ_{st} in Eq. 5;
k_1, k_2 = dimensionless stiffness coefficients in Eq. 12;
k_{11}, k_{22}, k_{21} = dimensionless stiffness coefficients in Eqs. 10 and 11;
k_x, k_y = stiffness of springs for model in Fig. 9;
M = amplitude of overturning moment;
P = amplitude of horizontal force;
r_o = radius of disk;
u = amplitude of horizontal displacement of disk in direction of P;
u_{st} = static value of u, defined by Eq. 4;
$V_s = \sqrt{G/\rho}$ = speed of propagation of shear waves in halfspace;
ν = Poisson's ratio for halfspace material;
ρ = mass density of halfspace material;
$\sigma_1, \sigma_2, \sigma_3$ = complex stress functions related to contact stresses, Eqs. 17;
$\sigma_x, \sigma_y, \sigma_z$ = [illegible];
ϕ = [illegible];
ϕ_{st} = [illegible].

Journal of the
SOIL MECHANICS AND FOUNDATIONS DIVISION
Proceedings of the American Society of Civil Engineers

SIMPLIFIED PROCEDURE FOR EVALUATING SOIL LIQUEFACTION POTENTIAL

By H. Bolton Seed,[1] M. ASCE and Izzat M. Idriss,[2] A. M. ASCE

Catastrophic failures in recent earthquakes have provided a sobering reminder that liquefaction of sandy soils as a result of earthquake ground shaking poses a major threat to the safety of civil engineering structures. Major landslides (25), lateral movements of bridge supports (6,24), settling and tilting of buildings (19,26), and failure of waterfront retaining structures (1,8,30) have all been observed in recent years as a result of this phenomenon and efforts have been increasingly directed to the development of methods of evaluating the liquefaction potential of soil deposits. It is the purpose of the present paper to describe a simplified procedure for evaluating liquefaction potential and to compare the results obtained by the method with a number of cases in which liquefaction is known either to have occurred, or not occurred in the field.

It should be noted at the outset that the term liquefaction as used herein describes a phenomenon in which a cohesionless soil loses strength during an earthquake and acquires a degree of mobility sufficient to permit movements ranging from several feet to several thousand feet. When the term was originally introduced it was intended to describe a phenomenon in which a soil would undergo large movements, as in flow slides, with little or no resistance to movements. However failures due to limited movements of several feet in recent earthquakes have been attributed to liquefaction. While the term cyclic mobility might be more appropriate to describe this type of soil behavior, the broader use of the term liquefaction is adopted in the following pages.

In addition, considerations of liquefaction are limited to cases of relatively level ground where the response of the soil to stresses induced by an earth-

Discussion open until February 1, 1972. To extend the closing date one month, a written request must be filed with the Executive Director, ASCE. This paper is part of the [illegible] Journal of the Soil Mechanics and Foundations Division, Proceedings of the American Society of Civil Engineers, Vol. 97, No. SM9, September, 1971. Manuscript was submitted for review for possible publication on January [illegible], 1971.

quake is not further complicated by the presence of initial horizontal shear stresses due to the proximity of significant surface irregularities.

FACTORS KNOWN TO INFLUENCE LIQUEFACTION POTENTIAL

Both laboratory investigations and observations of field performance have shown that the liquefaction potential of a soil deposit to earthquake motions depends on the characteristics of the soil, the initial stresses acting on the soil and the characteristics of the earthquake involved. The significant factors include: (1) Soil Type; (2) relative density or void ratio; (3) initial confining pressure; (4) intensity of ground shaking; and (5) duration of ground shaking.

Soil Type.—For cohesionless soils, the soil type is perhaps most easily characterized by the grain size distribution. There is some evidence to show that uniformly graded materials are most susceptible to liquefaction than well-graded materials [Ross, et al. (24); Lee and Fitton (16)] and that for uniformly graded soils, fine sands tend to liquefy more easily than do coarse sands, gravelly soils, silts, or clays (16). In a study of bridge foundation displacements in the Alaska earthquake, for example, Ross, et al. noted that there were no cases of bridge damage due to this cause for structures supported on gravels, but there were many cases of damage for bridges supported on sands. Again in the Fukui earthquake, Kishida (11) notes that liquefaction occurred at a site where the upper 15 ft consisted of medium sand, but there was no liquefaction at an adjacent site where the soil in this depth range was a sandy silt. These field observations are supported by the results of laboratory cyclic load tests on a wide range of materials (16).

Relative Density or Void Ratio.—Since the classical work of Casagrande (2) on the volume changes accompanying shear deformations in cohesionless soils, it has been generally recognized that the susceptibility of a given soil to liquefaction will be determined to a high degree by its void ratio or relative density. In any given earthquake loose sands may liquefy but the same materials in a denser condition may not.

In the city of Niigata, Japan in 1964, for example, liquefaction was extensive where the relative density of the sand was about 50 %, but it did not develop in areas where the relative density exceeded about 70 %. Laboratory test data of all types shows the important influence of this factor on soil behavior.

Initial Confining Pressure.—There is considerable evidence to show that under earthquake loading conditions, in contrast to flow-slide susceptibility under static load conditions, the liquefaction potential of a soil is reduced by an increase in confining pressure. Laboratory tests by numerous investigators (4,5,16,17,18,21,27) have shown that for a given initial density, the stress required to initiate liquefaction under cyclic load conditions increases with the initial confining pressure. The effect was also shown in the field during the Niigata earthquake where soil under a 9 ft fill remained stable, but similar soils surrounding the fill liquefied extensively (26).

The Intensity of Ground Shaking.—For a soil in a given condition and under a given confining pressure, the vulnerability to liquefaction during an earthquake depends on the magnitude of the stresses or strains induced in it by the earthquake; these in turn are related to the intensity of ground shaking. The significance of the applied stresses has been shown by many laboratory investigations, but the important effect of ground shaking intensity in the field is well illustrated by the soil behavior at Niigata in Japan. Records of earthquakes for this city extend back over a period exceeding 1,000 yr, and estimated values of maximum ground accelerations for earthquakes affecting the city in the past 370 yr are shown in Fig. 1. These values were determined from the relationships between earthquake magnitude, distance from source of energy release and maximum ground accelerations suggested by Housner (9) with appropriate corrections for the effect of local soil conditions based on the recorded ground acceleration of 0.16g in the 1964 earthquake. Magnitudes and epicenter locations for the earthquakes affecting Niigata have been presented by Kawasumi (10).

It may be seen in Fig. 1 that although the relatively loose sands in Niigata have been shaken by 25 earthquakes in the past 370 yr, historical records show only three occasions on which liquefaction has been reported in or near Niigata itself; on these occasions the estimated ground accelerations were in

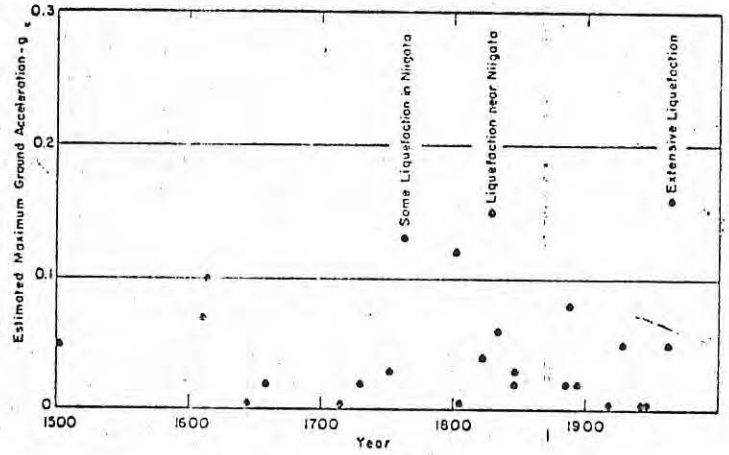

FIG. 1.—ESTIMATED MAXIMUM GROUND ACCELERATION IN NIIGATA

excess of 0.13g, culminating with the extensive liquefaction in 1964 when ground accelerations had their probable maximum value of 0.16g. Of special significance, however, is the fact that in 22 other earthquakes producing estimated ground accelerations ranging from 0.005g to 0.12g, there was no indication of any soil liquefaction in the city [Kawasumi (10)]. The intensity of ground motions must thus be considered an important factor in evaluating soil liquefaction potential.

Duration of Ground Shaking.—The duration of ground shaking is a significant factor in determining liquefaction potential because it determines in a general way the number of significant stress or strain cycles to which a soil is subjected. All laboratory studies of soil liquefaction under cyclic loading conditions show that for any given stress or strain level, the onset of liquefaction depends on the application of a requisite number of stress or strain cycles. In the field, the importance of this is perhaps best illustrated by the landslides which were triggered by liquefaction in Anchorage during the

Alaska earthquake of 1964. These slides did not occur until about 90 sec after the earthquake motions started (22) indicating the need for development of sufficient stress cycles to induce liquefaction and instability. Clearly if the duration of ground shaking had been only 45 sec, no liquefaction or soil instability would have developed.

GENERAL METHOD OF EVALUATING LIQUEFACTION POTENTIAL

In view of the evidence that the 2 forementioned five factors have a significant influence on the liquefaction potential of any soil deposit, it is apparent that any method for evaluating liquefaction potential should take these factors into account. Accordingly, Seed and Idriss (26) proposed a general method for evaluating liquefaction potential involving the following steps:

1. After establishing the soil conditions and the design earthquake, determine the time history of shear stresses induced by the earthquake ground motions at different depths within the deposit.
2. By appropriate weighting of the stress levels involved in the various stress cycles throughout the earthquake, convert the stress history into an equivalent number of uniform stress cycles and plot the equivalent uniform stress level as a function of depth as shown in Fig. 2. By this means the intensity of ground shaking, the duration of shaking, and the variation of shear stress with depth within the deposit are taken into account.
3. By means of available field data or laboratory soil tests on representative samples, conducted under various confining pressures, determine the cyclic shear stresses which would have to be developed at various depths to cause liquefaction in the same number of stress cycles as that determined in step 2 to be representative of the particular earthquake under consideration. Either cyclic load triaxial compression tests, or cyclic load simple shear tests may be used for this purpose. The interpretation of the test data to determine the stress conditions causing liquefaction in the field and the availability of field data have been presented elsewhere [Seed and Peacock (29)]. However in this way, the soil type, the in-place condition and the initial effective stress condition may be appropriately taken into account; the stresses required to cause failure may then be plotted as a function of depth as shown in Fig. 2.
4. By comparing the shear stresses induced by the earthquake with those required to cause liquefaction, determine whether any zone exists within the deposit where liquefaction can be expected to occur (induced stresses exceed those causing failure). In applying the method, the stress history at various depths in a deposit can best be determined by a ground response analysis (26), possibly conducted in steps to take into account the changing deformation characteristics of the soil as the pore pressures built up (28). In most cases this latter refinement is unnecessary because the soil properties do not change appreciably until liquefaction is imminent. Even so, a ground response analysis may involve techniques, skills and equipment which are not readily available. In addition, the conduct of cyclic load tests may present difficulties.

Accordingly, in applying the method over a period of time, simplified techniques have been developed for evaluating induced stresses and soil charac-

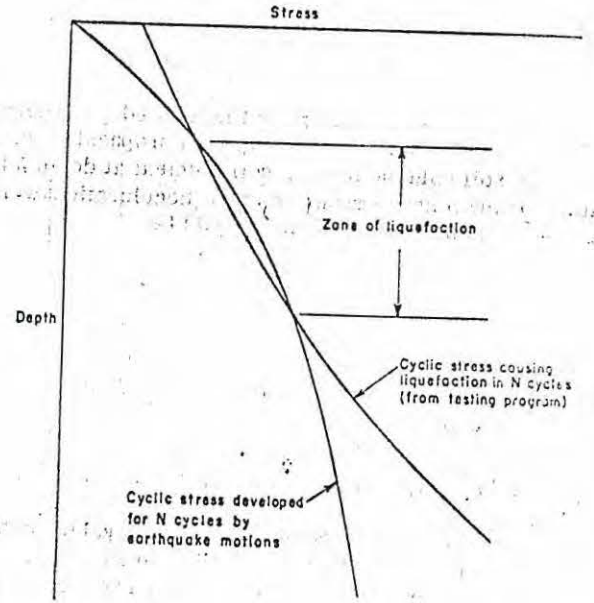

FIG. 2.—METHOD OF EVALUATING LIQUEFACTION POTENTIAL

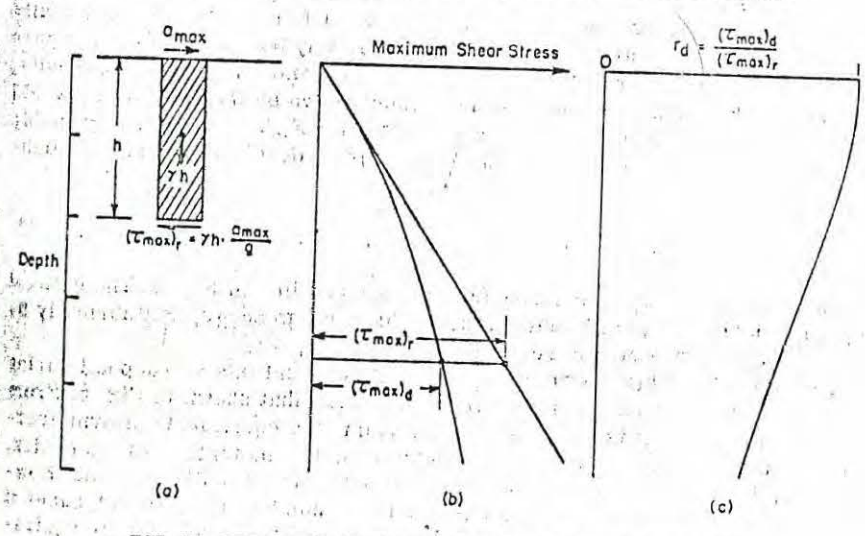

FIG. 3.—DETERMINATION OF MAXIMUM SHEAR STRESS

teristics which are sufficiently accurate for many practical purposes. These techniques are described herein.

SIMPLIFIED PROCEDURE FOR EVALUATING STRESSES INDUCED BY EARTHQUAKE

The shear stresses developed at any point in a soil deposit during an earthquake appear to be due primarily to the upward propagation of shear waves in the deposit. If the soil column above a soil element at depth h behaved as a rigid body and the maximum ground surface acceleration were a_{max}, the maximum shear stress on the soil element would be

$$(\tau_{max})_r = \frac{\gamma h}{g} a_{max} \quad \ldots\ldots (1)$$

in which γ = the unit weight of the soil [see Fig. 3(*a*)]. Because the soil column behaves as a deformable body, the actual shear stress at depth h, $(\tau_{max})_d$, as determined by a ground response analysis will be less than $(\tau_{max})_r$ and might be expressed by

$$(\tau_{max})_d = r_d \, (\tau_{max})_r \quad \ldots\ldots (2)$$

in which r_d = a stress reduction coefficient with a value less than 1. The variations of $(\tau_{max})_r$ and $(\tau_{max})_d$ will typically have the form shown in Fig. 3(*b*) and in any given deposit, the value of r_d will decrease from a value of 1 at the ground surface to much lower values at large depths, as shown in Fig. 3(*c*).

Computations of the value of r_d for a wide variety of earthquake motions and soil conditions having sand in the upper 50 ft have shown that r_d falls within the range of values shown in Fig. 4. It may be seen that in the upper 30 ft or 40 ft the scatter of the results is not great and for any of the deposits, the error involved in using the average values shown by the dashed line would generally be less than about 5 %. Thus to depths of about 40 ft, a reasonably accurate assessment of the maximum shear stress developed during an earthquake can be made from the relationship

$$\tau_{max} = \frac{\gamma h}{g} a_{max} \, r_d \quad \ldots\ldots (3)$$

in which values of r_d are taken from the dashed line in Fig. 4. The critical depth for development of liquefaction, if it is going to occur, will normally be in the depth covered by this relationship.

The actual time-history of shear stress at any point in a soil deposit during an earthquake will have an irregular from such as that shown in Fig. 5. From such relationships it is necessary to determine the equivalent uniform average shear stress. By appropriate weighting of the individual stress cycles, based on laboratory test data, this determination can readily be made. However after making these determinations for a number of different cases it has been found that with a reasonable degree of accuracy, the average equivalent uniform shear stress, τ_{av}, is about 65 % of the maximum shear stress, τ_{max}. Combining this result with the preceding expression for τ_{max} it follows that for practical purposes, the average cyclic shear stress may be

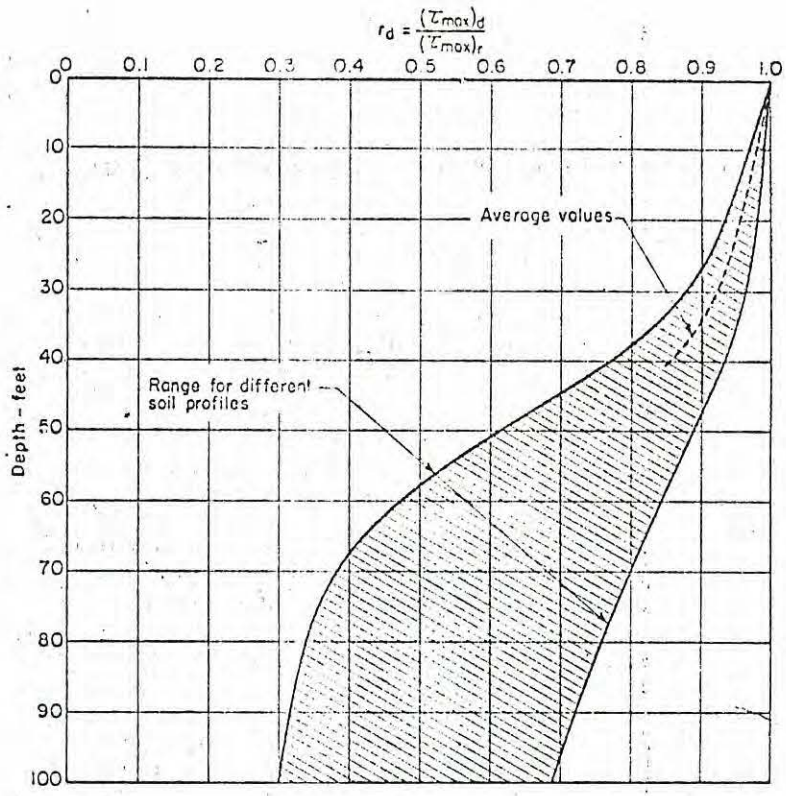

FIG. 4.—RANGE OF VALUES OF r_d FOR DIFFERENT SOIL PROFILES

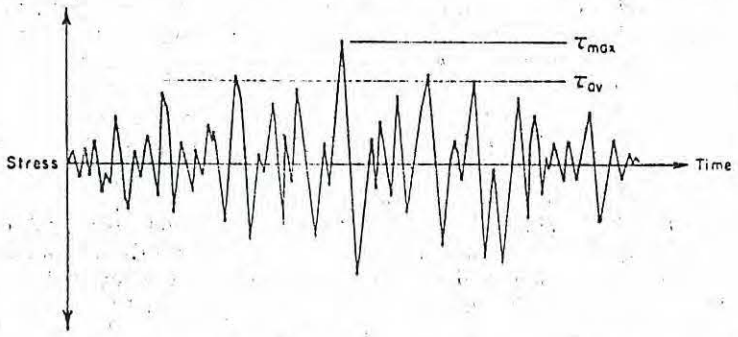

FIG. 5.—TIME HISTORY OF SHEAR STRESSES DURING EARTHQUAKE

determined by

$$\tau_{av} \simeq 0.65 \times \frac{\gamma h}{g} a_{max} \times r_d \quad \ldots\ldots\ldots\ldots\ldots\ldots\ldots\ldots\ldots\ldots (4)$$

The appropriate number of significant stress cycles N_c will depend on the duration of ground shaking, and thus on the magnitude of the earthquake. Representative numbers of stress cycles are

Earthquake Magnitude	Number of Significant Stress Cycles, N_c
7	10
7-1/2	20
8	30

The use of these values together with stresses determined from Eq. 4, provides a simple procedure for evaluating the stresses induced at different depths by any given earthquake for which the maximum ground surface acceleration is known.

SIMPLIFIED PROCEDURE FOR EVALUATING STRESSES CAUSING LIQUEFACTION

Determination of the cyclic shear stresses causing liquefaction of a given soil in a given number of stress cycles may be made either on the basis of the stress conditions known to have caused liquefaction of sands in previous earthquakes (29), or by means of an appropriate laboratory test program. Because available field data are somewhat generalized with respect to sand types and earthquake duration, a laboratory test program using cyclic loading triaxial compression tests is often preferred. The results of a number of such investigations on soils with different grain sizes, represented by the mean grain size, D_{50}, and at a relative density of 50 % are summarized in Figs. 6 and 7 (29). The results of these tests are expressed in terms of the stress ratio $\sigma_{dc}/(2\sigma_a)$ causing liquefaction in 10 cycles and 30 cycles, where σ_{dc} is the cyclic deviator stress and σ_a is the initial ambient pressure under which the sample was consolidated. Although the tests were performed by different investigators, it may be seen that there is a reasonable degree of consistency in the results, suggesting that these data may be used to estimate the liquefaction characteristics of other sands from a knowledge of the mean grain size, D_{50}. The stresses required to cause liquefaction for sands at other relative densities may be estimated from the fact that for relative densities up to about 80 %, the shear stress required to cause initial liquefaction is approximately proportional to the relative density.

Also shown in Figs. 6 and 7 are the values of the stress ratio τ/σ'_o causing liquefaction under field conditions, estimated from the results of simple shear tests; τ is the shear stress developed on a horizontal plane and σ'_o is the initial effective overburden pressure. It may be seen that the field value of τ/σ'_o is less than the corresponding value of $\sigma_{dc}/(2\sigma_a)$. However the two stress ratios may be related by

$$\left(\frac{\tau}{\sigma'_o}\right)_l = \left(\frac{\sigma_{dc}}{2\sigma_a}\right)_l c_r \quad \ldots\ldots\ldots\ldots\ldots\ldots\ldots\ldots\ldots\ldots (5)$$

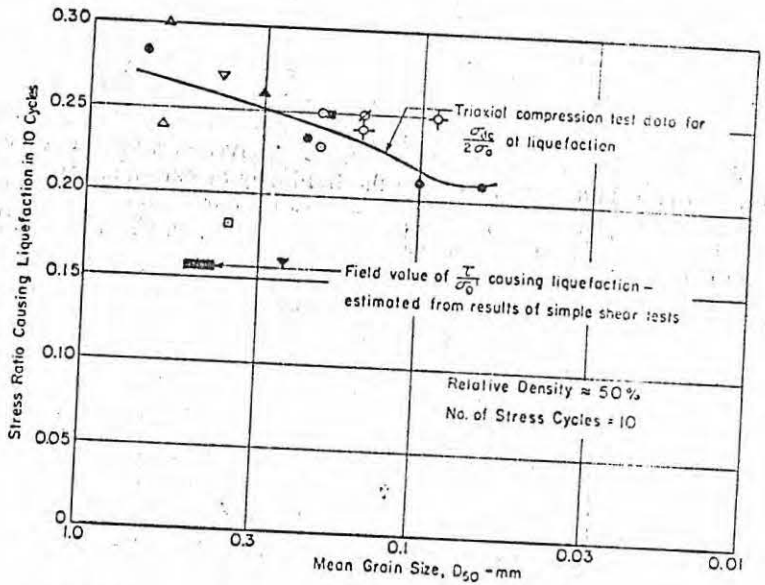

FIG. 6.—STRESS CONDITIONS CAUSING LIQUEFACTION OF SANDS IN 10 CYCLES

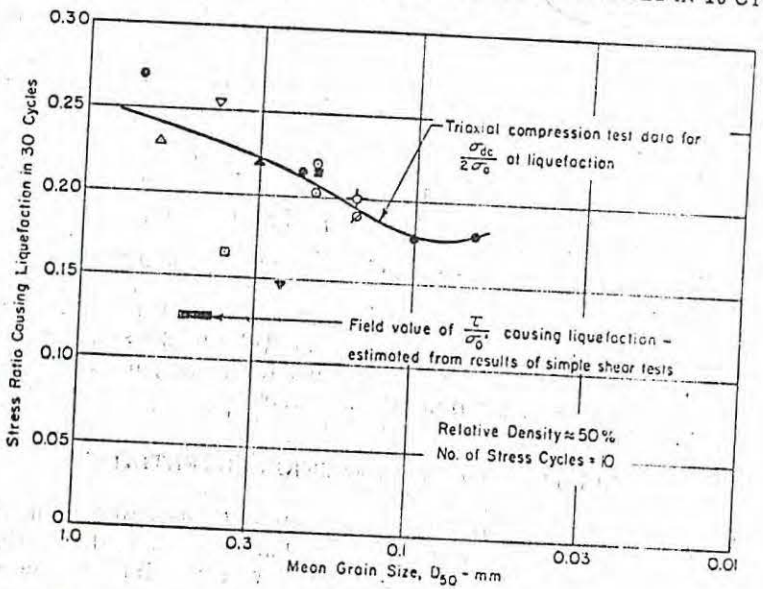

FIG. 7.—STRESS CONDITIONS CAUSING LIQUEFACTION OF SANDS IN 30 CYLES

in which c_r = a correction factor to be applied to laboratory triaxial test data to obtain the stress conditions causing liquefaction in the field. Detailed consideration of the stress conditions in triaxial compression test specimens and the limitations of the test itself have led to the suggestion that appropriate values of c_r vary with relative density approximately as shown in Fig. 8 (29). Thus the test data in Figs. 6 and 7 together with the values of c_r in Fig. 8 provide a simple means for assessing the stress conditions likely to cause liquefaction of different soils in the field. For a given soil at a relative D_r, the stress ratio causing liquefaction in the field may be estimated from

$$\left(\frac{\tau}{\sigma_o'}\right)_{lD_r} \simeq \left(\frac{\sigma_{dc}}{2\sigma_a}\right)_{l50} c_r \frac{D_r}{50} \quad \ldots\ldots (6)$$

in which the suffixes D_r and 50 denote relative densities of D_r and 50, respec-

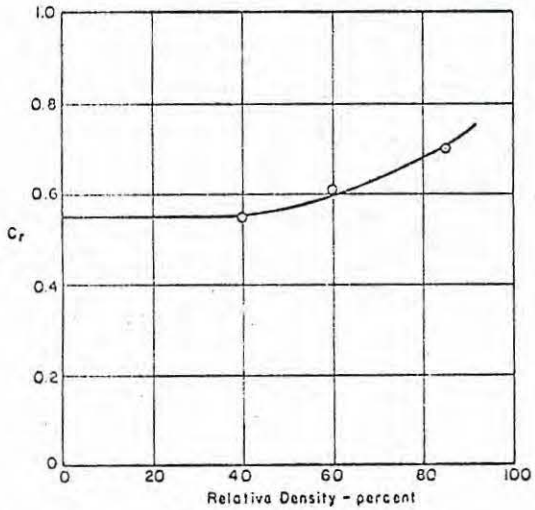

FIG. 8.—RELATIONSHIP BETWEEN c_r AND RELATIVE DENSITY

tively, and values of $[\sigma_{dc}/(2\sigma_a)]_{l50}$ are taken from Figs. 6 and 7. On specific projects it may often be desirable to perform cyclic load tests to determine the stress conditions causing liquefaction but for many purposes the use of Eq. 6 or available field data (29) may be adequate.

EVALUATION OF LIQUEFACTION POTENTIAL

In order to evaluate the liquefaction potential of a deposit it is necessary to determine whether the shear stress induced at any depth by the earthquake, determined from Eq. 4, is sufficiently large to cause liquefaction at that depth, as indicated by the relationship in Eq. 6. For deposits in which the water table is at a depth of 0 ft to 10 ft, the critical depth will often be about 20 ft and for those where the water table depth is about 15 ft, the critical depth may be about 30 ft. Thus the evaluation can often be made simply for a

representative element at one of these depths.

Consider for example, a deposit of sand for which $D_{50} \simeq 0.2$ mm, the water table is 5 ft below the ground surface and which is subjected to ground shaking by a magnitude 7 earthquake. The average shear stress induced for about 10 cycles will be determined from Eq. 4. At a depth of 20 ft, $r_d \simeq 0.95$ (see Fig. 4) giving

$$\tau_{av} \simeq 0.65 \times 0.95 \times \frac{\gamma h}{g} a_{max} \quad \ldots\ldots (7)$$

If the shear stress required to cause initial liquefaction in 10 cycles is τ_{l10}, it follows from Eq. 6

$$\frac{\tau_{l10}}{\sigma_o'} \simeq \left(\frac{\sigma_{dc}}{2\sigma_a}\right)_{l50} \frac{D_r}{50} c_r \quad \ldots\ldots (8)$$

However for a soil with $D_{50} \simeq 0.2$ mm, the data in Fig. 6 show that

$$\left(\frac{\sigma_{dc}}{2\sigma_a}\right)_{l50} \simeq 0.24 \quad \ldots\ldots (9)$$

giving $\tau_{l10} \simeq 0.24\, \sigma_o' \frac{D_r}{50} c_r \quad \ldots\ldots (10)$

The sand will develop initial liquefaction in 10 cycles if

$$\tau_{av} = \tau_{l10} \quad \ldots\ldots (11)$$

i.e. $0.65 \times 0.95 \times \frac{\gamma h}{g} a_{max} = 0.24\, \sigma_o' \frac{D_r}{50} c_r \quad \ldots\ldots (12)$

$$\text{or } \frac{a_{max}}{g} \simeq \frac{0.24}{0.65 \times 0.95 \times 50} \frac{\sigma_o'}{\gamma h} c_r D_r \simeq 0.0078 \frac{\sigma_o'}{\gamma h} c_r D_r \quad \ldots\ldots (13)$$

For a water table 5 ft below the ground surface and a soil element at a depth of 20 ft

$$\gamma h \simeq 20 \times 112 \simeq 2{,}240 \text{ psf} \quad \ldots\ldots (14)$$

$$\sigma_o' \simeq 5 \times 112 + 15 \times 50 \simeq 1{,}310 \text{ psf} \quad \ldots\ldots (15)$$

$$\text{Thus } \frac{a_{max}}{g} \simeq 0.0078 \times \frac{1{,}310}{2{,}240} c_r D_r \simeq 0.0046\, c_r D_r \quad \ldots\ldots (16)$$

The relationship between a_{max} and D_r indicated by this equation may be evaluated as follows:

D_r	c_r (from Fig. 8)	$a_{max}/g = 0.0046\, c_r D_r$
30	0.55	0.076
40	0.55	0.100
50	0.57	0.131
60	0.60	0.166
70	0.64	0.205
80	0.68	0.250

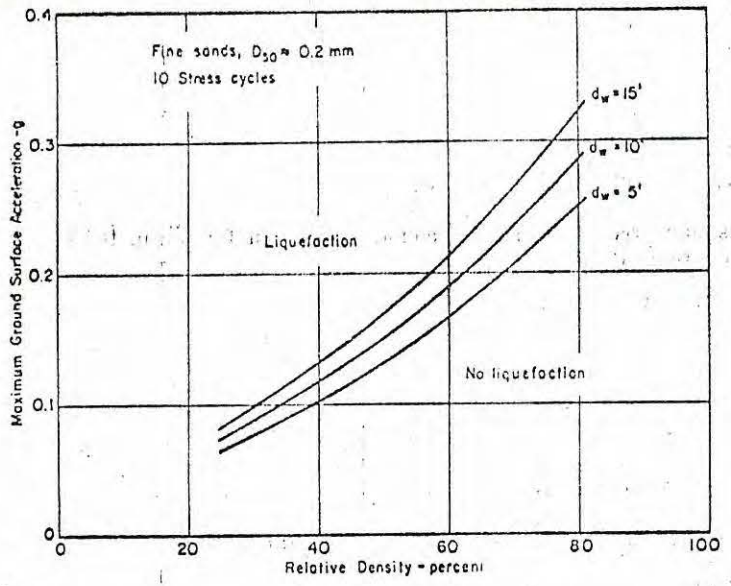

FIG. 9.—EVALUATION OF LIQUEFACTION POTENTIAL FOR FINE SAND—10 STRESS CYCLES

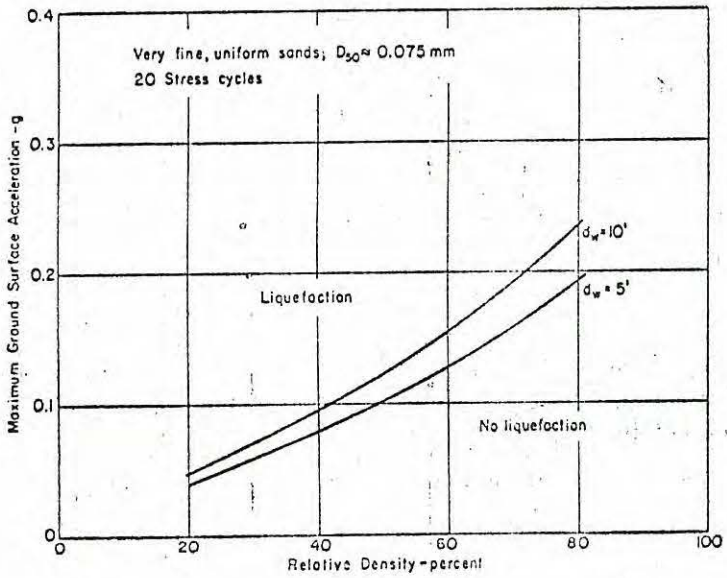

FIG. 10.—EVALUATION OF LIQUEFACTION POTENTIAL FOR VERY FINE SAND—20 STRESS CYCLES

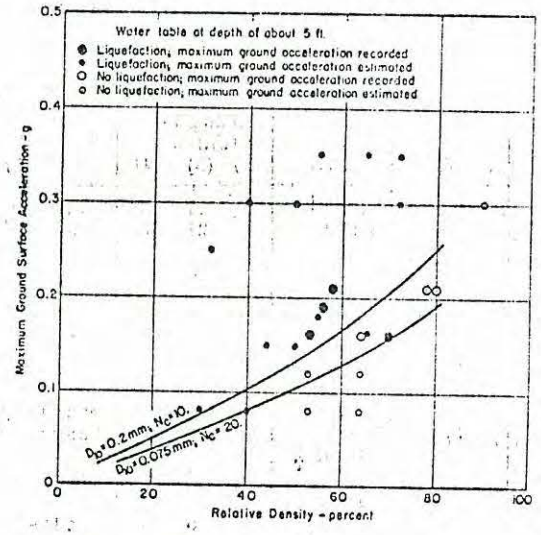

FIG. 11.—EVALUATION OF LIQUEFACTION POTENTIAL FOR FINE SANDS—WATER TABLE 5 FT BELOW GROUND SURFACE

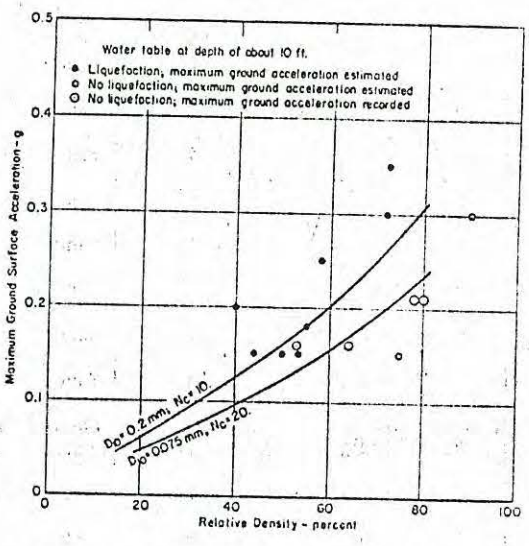

FIG. 12.—EVALUATION OF LIQUEFACTION POTENTIAL FOR FINE SANDS—WATER TABLE 10 FT BELOW GROUND SURFACE

TABLE 1.—SITE CONDITIONS AND EARTHQUAKE DATA FOR KNOWN CASES OF LIQUEFACTION AND NONLIQUEFACTION

Earthquake (1)	Date (2)	Magnitude (3)	Site (4)	Approximate distance from source of energy release, in miles (5)	Soil type (6)	Depth of water table, in feet (7)	Critical depth, in feet (8)	Average penetration resistance at critical depth $\bar{N}$ (9)	Relative density, as a percentage (10)	Maximum ground surface acceleration, in units of g (11)	Duration of shaking, in seconds (12)	Field behavior (13)	References (14)
Niigata	1802	6.6	Niigata	24	Sand	3	20	6	53	0.12	≈20	No liquefaction	Kawasumi (10)
Niigata	1802	6.6	Niigata	24	Sand	3	20	12	64	0.12	≈20	No liquefaction	Seed and Idriss (26)
Niigata	1887	6.1	Niigata	29	Sand	3	20	6	53	0.08	≈12	No liquefaction	Kawasumi (10)
Niigata	1887	6.1	Niigata	29	Sand	3	20	12	64	0.08	≈12	No liquefaction	Seed and Idriss (26)
Mino Owari	1891	8.4	Ogaki	20	Sand	3	45	17	65	≈0.35	≈75	Liquefaction	Kishida (12)
Mino Owari	1891	8.4	Ginan West	20	Sand	6	30	10	55	≈0.35	≈75	Liquefaction	Kishida (12)
Mino Owari	1891	8.4	Unuma	20	Sand and gravel	6	25	19	75	≈0.35	≈75	No liquefaction	Kishida (12)
Mino Owari	1891	8.4	Ogase Pond	20	Sand	8	20	16	72	≈0.35	≈75	Liquefaction	Kishida (12)
Santa Barbara	1925	6.3	Sheffield Dam	7	Sand	≈15	25	—	40	≈0.2	15	Liquefaction	Seed et al. (28)
El Centro	1940	7.0	Brawley	5	Sand	≈15	≈15	—	58	≈0.25	30	Liquefaction	Ross (23)
El Centro	1940	7.0	All-Am. Canal	5	Sand	≈20	≈25	—	43	≈0.25	30	Liquefaction	Ross (23)
El Centro	1940	7.0	Solfatara Canal	5	Sand	5	≈20	—	32	≈0.25	30	Liquefaction	Ross (23)
Tohnankai	1944	8.3	Komei	100	Sand	5	13	4	40	≈0.08	≈70	Liquefaction	Kishida (12)
Tohnankai	1944	8.3	Meiko St.	100	Silt and sand	2	8	1	30	≈0.08	≈70	Liquefaction	Kishida (12)
Fukui	1948	7.2	Takaya	4	Sand	11	23	18	72	≈0.30	≈30	Liquefaction	Kishida (12)
Fukui	1948	7.2	Takaya	4	Sand	3	23	28	90	≈0.30	≈30	No liquefaction	Kishida (12)
Fukui	1948	7.2	Shonenji Temple	4	Sand	4	10	3	40	≈0.30	≈30	Liquefaction	Kishida (12)
Fukui	1948	7.2	Agr. Union	4	Sand and silt	3	20	5	50	≈0.30	≈30	Liquefaction	Kishida (12)
San Francisco	1957	5.5	Lake Merced	4	Sand	8	10	7	55	≈0.18	18	Liquefaction	Ross (23)
Chile	1960	8.4	Puerto Montt	≈70	Sand	12	15	6	50	≈0.15	≈75	Liquefaction	Lee (15)
Chile	1960	8.4	Puerto Montt	≈70	Sand	12	15	8	55	≈0.15	≈75	Liquefaction	Lee (15)
Chile	1960	8.4	Puerto Montt	≈70	Sand	12	20	18	75	≈0.15	≈75	No liquefaction	Lee (15)
Niigata	1964	7.5	Niigata	32	Sand	3	20	6	53	0.16	40	Liquefaction	Seed and Idriss (26)
Niigata	1964	7.5	Niigata	32	Sand	3	25	15	70	0.16	40	Liquefaction	Kishida (11)
Niigata	1964	7.5	Niigata	32	Sand	3	20	12	64	0.16	40	No liquefaction	Seed and Idriss (26)
Niigata	1964	7.5	Niigata	32	Sand	12	25	6	53	0.16	40	No liquefaction	Seed and Idriss (26)
Alaska	1964	8.3	Snow River	60	Sand	0	20	5	50	≈0.15	180	Liquefaction	Ross et al. (24)
Alaska	1964	8.3	Snow River	60	Sand	8	20	5	44	≈0.15	180	Liquefaction	Ross et al. (24)
Alaska	1964	8.3	Quartz Creek	70	Sandy gravel	0	≈25	40-80	100	≈0.12	180	No liquefaction	Ross et al. (24)

TABLE 1.—

(1)	(2)	(3)	(4)	(5)	(6)	(7)
Alaska	1964	8.3	Scott Glacier	55	Sand	0
Alaska	1964	8.3	Valdez	35	Sand and gravel	5
Tokachioki	1968	7.8	Hachinohe	45 to 110	Sand	3
Tokachioki	1968	7.8	Hachinohe	45 to 110	Sand	3
Tokachioki	1968	7.8	Hachinohe	45 to 110	Sand	5
Tokachioki	1968	7.8	Hakodate	100	Sand	3

and the relationship can be plotted as shown in Fig. 9. If, for any given value of maximum ground acceleration, the relative density of the deposit exceeds the value indicated by this relationship, liquefaction would not be expected to occur, and vice versa. Relationships computed following the same procedure for water table depths of 10 ft and 15 ft are also plotted in Fig. 9, indicating the lower degree of liquefaction potential resulting from a greater depth of water table.

Similar computations can readily be made for other soil types, depths of water table and number of stress cycles. Soils having the greatest susceptibility to liquefaction appear to be very fine uniform sands, with D_{50} of the order of 0.08 mm. For such materials the relationships between a_{max} and relative density for which initial liquefaction would just occur in an earthquake producing 20 stress cycles for different water table elevations are shown in Fig. 10.

In general when liquefaction of sands develops in the field, the mean grain size might be expected to range from 0.075 mm to about 0.2 mm and the number of stress cycles from 10 to 20. Thus the boundaries between conditions which do and do not liquefy might normally be expected to be within the range by the conditions: $D_{50} \simeq 0.075$ mm; $N_c = 20$; $D_{50} \simeq 0.2$ mm; $N_c = 10$. The computed relationships between relative density and maximum ground acceleration for which initial liquefaction will just occur for these conditions are plotted in Figs. 11 and 12 for water table depths of 5 ft and 10 ft, respectively. For earthquakes exceeding about Magnitude 7 and appropriate water table depths, it might therefore be expected that combinations of relative density and maximum ground surface acceleration falling above the upper curve ($D_{50} \simeq 0.2$ mm; $N_c = 10$) in Figs. 11 and 12 would often cause liquefaction; combinations falling below the lower curve ($D_{50} \simeq 0.075$ mm; $N_c = 20$) would usually be safe against liquefaction; while combinations falling between the curves might cause liquefaction or not, depending on the particular combination of conditions involved. It is believed that charts of this type can provide a useful guide in the evaluation of soil liquefaction potential during earthquakes.

COMPARISON OF LIQUEFACTION POTENTIAL EVALUATIONS WITH FIELD BEHAVIOR

The only reliable method for determining the usefulness of any method of evaluating liquefaction potential is by comparing its results with the known performance of soils in the field. Accordingly a compilation has been made of a number of cases in which sand deposits have, or have not liquefied during earthquakes. The soil conditions, ground motions and field behavior in these cases are summarized in Table 1.

CONTINUED

(8)	(9)	(10)	(11)	(12)	(13)	(14)
≃20	10	65	≃0.16	180	Liquefaction	Ross et al. (24)
≃20	13	68	≃0.25	180	Liquefaction	Coulter and Migliaccio (3)
12	14	78	0.21	45	No liquefaction	Ohsaki (20)
12	6	58	0.21	45	Liquefaction	Ohsaki (20)
10	15	80	0.21	45	No liquefaction	Ohsaki (20)
15	6	55	0.18	45	Liquefaction	Kishida (13)

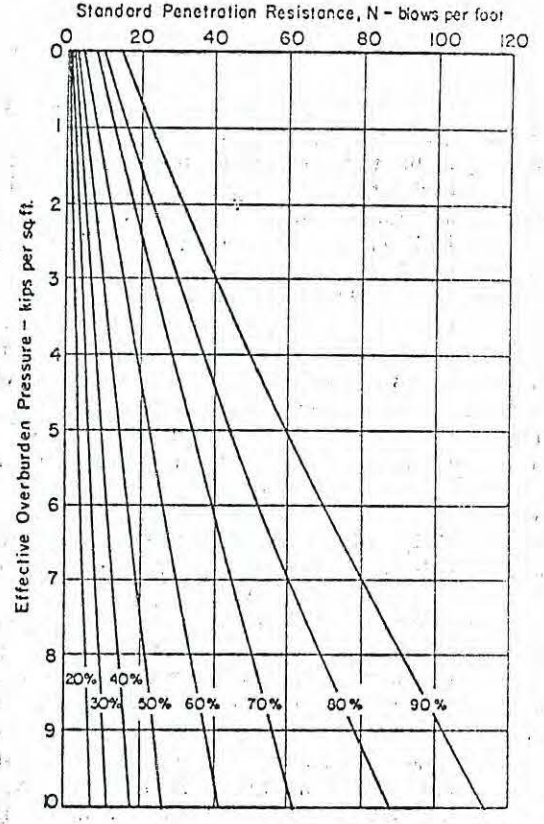

FIG. 13.—RELATIONSHIP BETWEEN STANDARD PENETRATION RESISTANCE, RELATIVE DENSITY AND EFFECTIVE OVERBURDEN PRESSURE (AFTER GIBBS AND HOLTZ)

In most cases no direct measurement of relative density was made but data were available concerning the standard penetration resistance of the deposits. In these cases the in-situ relative density was determined from the relationship between relative density, penetration resistance and effective overburden pressure proposed by Gibbs and Holtz (7). This correlation is presented in Fig. 13.

In addition, measurements of maximum ground accelerations were available for only a few cases. Thus in most cases it was necessary to estimate the maximum ground surface accelerations from the approximate relationships between earthquake magnitude, distance from zone of energy release, and maximum ground acceleration proposed by Housner (9).

In this way, for locations where the water table was about 5 ft below the ground surface, it was possible to determine combinations of relative density and maximum ground surface acceleration for 15 cases where liquefaction is known to have occurred and eight cases where liquefaction did not develop. These cases are plotted in Fig. 11, larger symbols being used for cases where ground motion measurements were available and smaller symbols for cases where ground motions had to be estimated.

For locations where the water table was about 10 ft below the ground surface it was possible to determine combinations of relative density and maximum ground surface acceleration for eight cases where liquefaction is known to have occurred and six cases where liquefaction did not develop. These cases are plotted in Fig. 12.

It may be seen from Figs. 11 and 12 that the liquefaction behavior of soils in the field is in reasonably good agreement with the anticipated behavior determined by the simplified procedure for evaluating liquefaction potential. It appears therefore that evaluations of this type provide not only a convenient means of summarizing available knowledge of conditions causing liquefaction in the field in past earthquakes, but also of extending this information to different conditions of relative density and maximum ground accelerations.

COMPARISON OF LIQUEFACTION POTENTIAL EVALUATIONS WITH LIMITING CONDITIONS FOR LIQUEFACTION AT NIIGATA

In the Niigata earthquake of June 16, 1964, extensive liquefaction occurred in some parts of the city, but not in others. The maximum ground acceleration recorded in the city was 0.16*g*. Following the earthquake Japanese engineers made detailed studies to determine the differences in soil conditions between the heavy damage area where liquefaction occurred and the light damage area where liquefaction did not develop. It was concluded that the essential difference was a somewhat higher relative density, as evidenced by higher values of the standard penetration resistance, in the light damage area as compared with the heavy damage area. Independent studies by Kishida (11) and Koizumi (14) led to the delineation of boundaries, in terms of variations of penetration resistance with effective overburden pressure, between those soil conditions producing liquefaction and those for which liquefaction did not occur, (see Fig. 14).

It is interesting to compare these boundaries with those which might be determined by the simplified procedure for evaluating liquefaction potential. For the conditions at Niigata, the mean grain size for the soil ranged from

about 0.1 mm to 0.5 mm, the water table was about 5 ft below the ground surface, and the earthquake (Magnitude about 7.6) could be expected to produce about 20 significant stress cycles. Reference to Fig. 11 shows that for these conditions and a maximum ground surface acceleration of 0.16*g*, it would be necessary for the sand to have a relative density of about 72 % to be marginally safe against liquefaction. Thus the limiting conditions for no liquefaction to occur would be expected to correspond approximately with a relative density condition of about 72 % in the upper 30 ft. Combinations of effective overburden pressure and standard penetration resistance corresponding to this relative density may be read directly from Fig. 13, and they are plotted in Fig. 14. It may be seen that the boundary between zones of liquefaction and no liquefaction determined in this way is in reasonably good agreement with

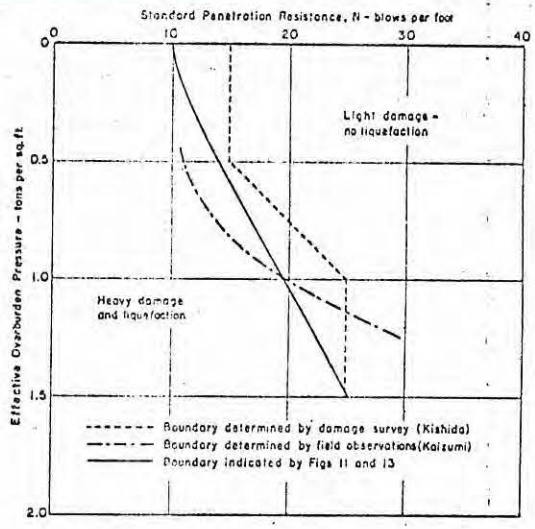

FIG. 14.—ANALYSIS OF LIQUEFACTION POTENTIAL AT NIIGATA FOR EARTHQUAKE OF JUNE 16, 1964

the boundaries determined by Kishida and Koizumi on the basis of field observations.

CHARTS FOR EVALUATING LIQUEFACTION POTENTIAL IN TERMS OF PENETRATION RESISTANCE

Both the simplified analysis procedure described previously and the data in Figs. 11 and 12 may readily be used to develop simple charts for the evaluation of liquefaction potential in terms of penetration resistance values. For example on the basis of the analytical and field data shown in Fig. 15 (reproduced from Fig. 11) it is very unlikely that combinations of maximum ground acceleration and relative density falling below line YY would cause liquefaction. Similarly it is highly probable that combinations of maximum ground acceleration and relative density falling above line XX would cause liquefaction of sands in which the depth of water table is about 5 ft. Thus for any given

value of maximum ground acceleration, it is possible to designate three ranges of relative densities: (1) A range in which liquefaction is very likely to occur; (2) a range in which liquefaction may or may not occur depending on the characteristics of the sand and the number of significant stress cycles produced by the earthquake or the earthquake magnitude (zone between XX and YY in Fig. 15); and (3) a range in which liquefaction is very unlikely to occur. For sites consisting of sands with the water table about 5 ft below the ground surface, the results in Fig. 15 would indicate the ranges shown in

TABLE 2.—VALUES OF RELATIVE DENSITY

Maximum ground surface acceleration (1)	Liquefaction very likely (2)	Liquefaction potential depends on soil type and earthquake magnitude (3)	Liquefaction very likely (4)
0.10g	$D_r < 33$	$33 < D_r < 54$	$D_r > 54$
0.15g	$D_r < 48$	$48 < D_r < 73$	$D_r > 73$
0.20g	$D_r < 60$	$60 < D_r < 85$	$D_r > 85$
0.25g	$D_r < 70$	$70 < D_r < 92$	$D_r > 92$

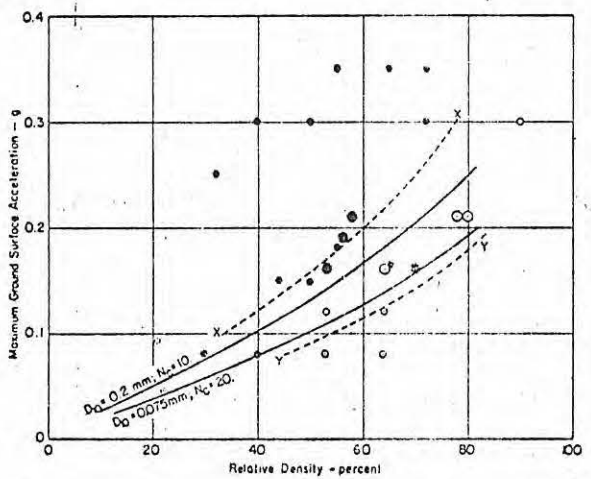

FIG. 15.—EVALUATION OF LIQUEFACTION POTENTIAL FOR SNADS—WATER TABLE 5 FT BELOW GROUND SURFACE

Table 2. The values of relative density listed in Table 2 can readily be converted to corresponding values of standard penetration resistance by means of the correlation shown in Fig. 13, thus leading to liquefaction potential evaluation charts such as those shown in Fig. 16. Charts for a water table depth of 10 ft are shown in Fig. 17 and similar charts for other depths of water table can readily be developed. However, it may be seen that the range of penetration resistance values in which the liquefaction potential depends on the soil type and the earthquake characteristics is considerable; for con-

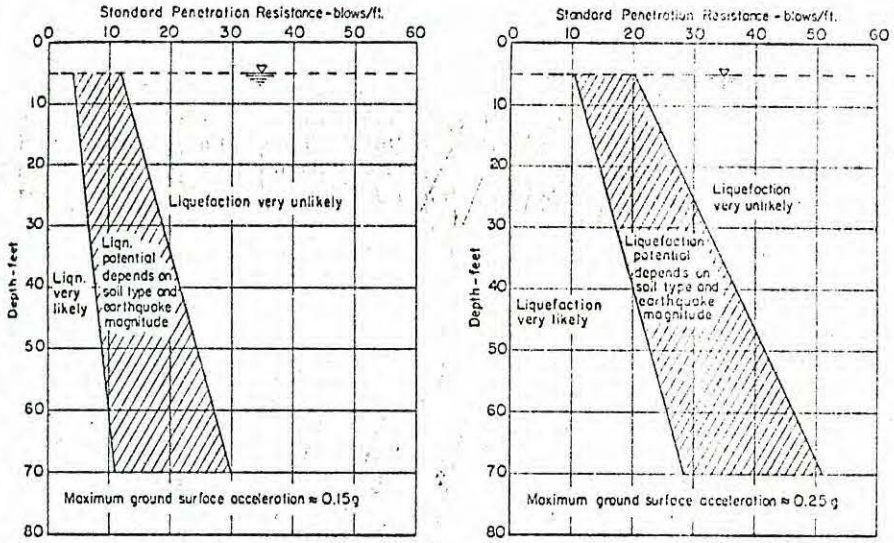

FIG. 16.—LIQUEFACTION POTENTIAL EVALUATION CHARTS FOR SANDS WITH WATER TABLE AT DEPTH OF ABOUT 5 FT

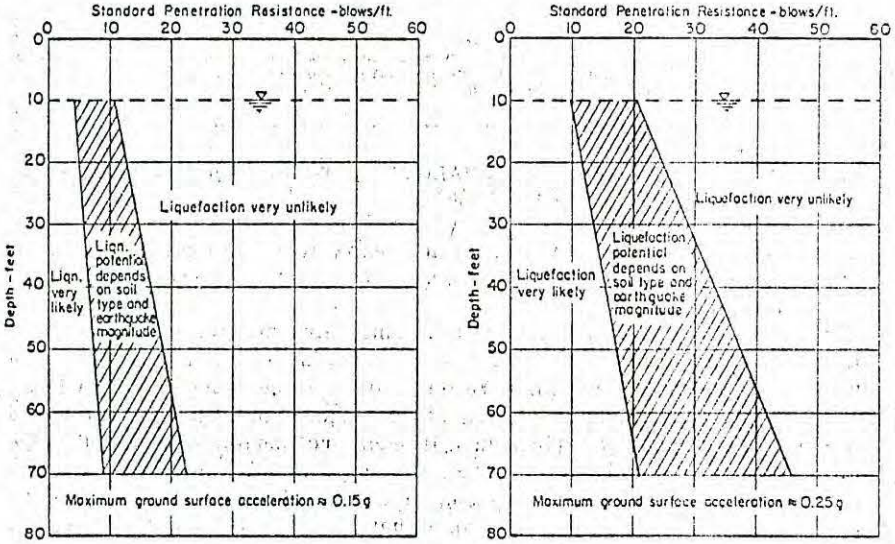

FIG. 17.—LIQUEFACTION POTENTIAL EVALUATION CHARTS FOR SANDS WITH WATER TABLE AT DEPTH OF ABOUT 10 FT

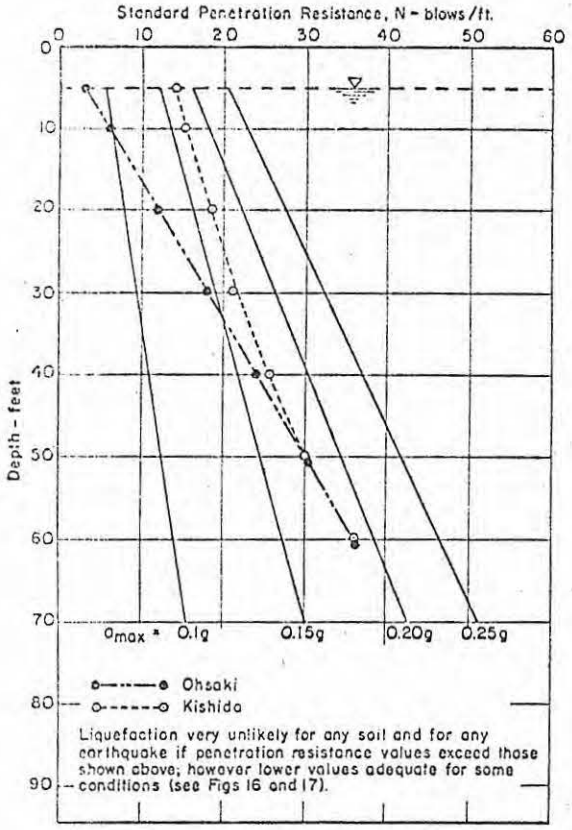

FIG. 18.—PENETRATION RESISTANCE VALUES FOR WHICH LIQUEFACTION IS UNLIKELY TO OCCUR UNDER ANY CONDITIONS

ditions within this range it would be necessary to make individual assessments of liquefaction potential for each site using the general procedure described previously.

The limiting values of penetration resistance for which liquefaction is very unlikely, as indicated by Table 2 and the results in Fig. 16, are compared in Fig. 18. Also shown in this figure are the limiting values suggested by Ohsaki (20) based on experiences in the Niigata earthquake and Kishida (12), based on a study of a number of earthquakes. It seems reasonable to expect that the limiting boundary would vary depending on the intensity of shaking as indicated by the results of this study and that the limiting values suggested by Ohsaki and Kishida are perhaps somewhat conservative for low intensity shaking and somewhat unconservative for strong intensity shaking.

CONCLUSIONS

An attempt has been made to identify some of the significant factors affecting the liquefaction (or cyclic mobility) potential of sands during earthquakes,

to present a simplified procedure for evaluating liquefaction potential which will take these factors into account, to assemble available field data concerning the liquefaction or nonliquefaction behavior of sands during earthquakes, and to compare these data with evaluations of performance made by the simplified procedure. It must be recognized that in any study of this type, a number of approximations must be made especially with regard to determination of relative densities and maximum ground accelerations in the field. However it is believed that even the limited available field data can provide a useful guide to the probable performance of other sand deposits, that the method of representing the data provides a useful framework for evaluating past experiences of sand liquefaction, and that the simplified procedure provides a reasonably good means for extending previous field observations to new situations. Where greater accuracy is justified, the simplified liquefaction evaluation procedure can readily be supplemented by test data on particular soils or by ground response analyses to provide more definitive evaluations. However it is believed that the simplified procedure will provide adequate assessments of liquefaction potential for many practical purposes.

ACKNOWLEDGMENTS

The investigation described in the preceding pages was performed as part of a study of "Soil and Foundation Response During Earthquakes," under the sponsorship of the National Science Foundation. The writers are most grateful for this support and for the assistance of P. Schnabel in making some of the computations required in the investigation.

APPENDIX I.—REFERENCES

1. Amano, Ryokichi, Azuma, Hisashi and Ishii, Yasumaru, "Ascismic Design of Quay Walls in Japan," *Proceedings*, 1st World Conference on Earthquake Engineering, Berkeley, Calif., 1956.
2. Casagrande, A., "Characteristics of Cohesionless Soils Affecting the Stability of Slopes and Earth Fills," *Journal*, Boston Society of Civil Engineers, Jan., 1936.
3. Coulter, H. W. and Migliaccio, R. R., "Effects of the Earthquake of March 27, 1964 at Valdez, Alaska," *Geological Survey Professional Paper 542-C*, U.S. Deparmtnet of the Interior, 1966.
4. Finn, W. D. Liam, Pickering, D. J. and Bransby, P. L., "Sand Liquefaction in Triaxial and Simple Shear Tests," *Soil Mechanics Research Report Series No. 11*, University of British Columbia, Vancouver, Canada, Aug., 1969.
5. Florin, V. A. and Ivanov, P. L., "Liquefaction of Saturated Sandy Soils," *Proceedings*, 5th International Conference on Soil Mechanics and Foundation Engineering, Paris, France, 1961.
6. Fukuoka, Masami, "Damage to Civil Engineering Structures," *Soil and Foundation*, Tokyo, Japan, Vol. VI, No. 2, March, 1966.
7. Gibbs, H. J. and Holtz, W. G., "Research on Determining the Density of Sand by Spoon Penetration Test," *Proceedings*, Fourth International Conference on Soil Mechanics and Foundations Engineering, Vol. I, pp. 35-39, 1957.
8. Hayashi, Satoshi, Kubo, Koichi and Nakase, Akio, "Damage to Harbour Structures by the Niigata Earthquake," *Soil and Foundation*, Tokyo, Japan, Vol. VI, No. 1, Jan., 1966.
9. Housner, George W., "Intensity of Earthquake Ground Shaking Near the Causative Fault,"

Proceedings of the 3rd World Conference on Earthquake Engineering, Auckland, New Zealand, 1964.
10. Kawasumi, Hirosi, "Historical Earthquakes in the Disturbed Area and Vicinity," *General Report on the Niigata Earthquake of 1964*, Electrical Engineering College Press, University of Tokyo, March, 1968.
11. Kishida, H., "Damage to Reinforced Concrete Buildings in Niigata City with Special Reference to Foundation Engineering," *Soil and Foundation*, Tokyo, Japan, Vol. VII, No. 1, pp. 71-88, 1966.
12. Kishida, Hideaki, "Characteristics of Liquefied Sands During Mino-Owari, Tohnankai and Fukui Earthquakes," *Soil and Foundation*, Vol. IX, No. 1, 1969.
13. Kishida, H., "Characteristics of Liquefaction of Level Sandy Ground During the Tokachioki Earthquake," *Soil and Foundation*, Tokyo, Japan, Vol. X, No. 2, June, 1970.
14. Koizumi, Y., "Change in Density of Sand Subsoil Caused by the Niigata Earthquake," *Soil and Foundantion*, Tokyo, Japan, Vol. VI, No. 2, pp. 38-44, March, 1966.
15. Lee, K. L., Private Communication, 1970.
16. Lee, K. L. and Fitton, J. A., "Factors Affecting the Cyclic Loading Strength of Soil," Vibration Effects of Earthquakes on Soils and Foundations, ASTM STP 450, American Society for Testing and Materials, 1969.
17. Lee, K. L. and Seed, H. B., "Cyclic Stresses Causing Liquefaction of Sand," *Journal of the Soil Mechanics and Foundations Division*, ASCE, Vol. 93, No. SM1, Proc. Paper 5058, Jan., 1967, pp. 47-70.
18. Maslov, N. N., "Questions of Seismic Stability of Submerged Sandy Foundations and Structures," *Proceedings*, 4th International Conference on Soil Mechanics and Foundations Engineering, London, England, 1957.
19. Ohsaki, Yorihiko, "Niigata Earthquakes, 1964 Building Damage and Soil Condition," *Soil and Foundation*, Tokyo, Japan, Vol. VI, No. 2, March 1966.
20. Ohsaki, Y., "Effects of Sand Compaction on Liquefaction During the Tokachioki Earthquake," *Soil and Foundation*, Tokyo, Japan, Vol. X, No. 2, June, 1970.
21. Peacock, William H. and Seed, H. Bolton, "Sand Liquefaction Under Cyclic Loading Simple Shear Conditions," *Journal of the Soil Mechanics and Foundations Division*, ASCE, Vol. 94, No. SM3, Proc. Paper 5957, May, 1968, pp. 689-708.
22. *Report on Anchorage Area Soil Studies, Alaska*, Shannon and Wilson, Inc., to U.S. Army Engineer District, Anchorage, Alaska, Seattle, Washington, 1964.
23. Ross, Grant A., "Case Studies of Soil Stability Problems Resulting from Earthquakes," thesis submitted to the University of California, at Berkeley, in 1968, in partial fulfillment of the requirements for the degree of Doctor of Philosophy.
24. Ross, Grant A., Seed, H. Bolton and Migliaccio, Ralph R. (1969) "Bridge Foundations in Alaska Earthquake," *Journal of the Soil Mechanics and Foundations Division*, ASCE, Vol. 95, No. SM4, Proc. Paper 6664, July, 1969, pp. 1007-1036.
25. Seed, H. Bolton, "Landslides During Earthquakes Due to LiqueFaction," *Journal of the Soil Mechanics and Foundations Division*, ASCE, Vol. 94, No. SM5, Proc. Paper 6110, Sept., 1968, pp. 1053-1122.
26. Seed, H. Bolton and Idriss, I. M., "Analysis of Soil Liquefaction: Niigata Earthquake," *Journal of the Soil Mechanics and Foundations Division*, ASCE, Vol. 93, No. SM3, Proc. Paper 4233, May, 1967, pp. 83-108.
27. Seed, H. Bolton and Lee, Kenneth L., "Liquefaction of Saturated Sands During Cyclic Loading," *Journal of the Soil Mechanics and Foundations Division*, ASCE, Vol. 92, No. SM6, Proc. Paper 4972, Nov., 1966, pp. 105-134.
28. Seed, H. Bolton, Lee, Kenneth L. and Idriss, I. M., "Analysis of Sheffield Dam Failure," *Journal of the Soil Mechanics and Foundations Division*, ASCE, Vol. 95, No. SM6, Proc. Paper 6906, Nov., 1969, pp. 1453-1490.
29. Seed, H. Bolton and Peacock, W. H., "Applicability of Laboratory Test Procedures for Measuring Soil Liquefaction Characteristics Under Cyclic Loading," Earthquake Engineering Research Center, *Report No. EERC 70-8*, Nov., 1970.
30. Seed, H. Bolton and Whitman, Robert V., "Design of Earth Retaining Structures for Dynamic Loads," *Proceedings of the Specialty Conference on Lateral Stresses in the Ground and Design of Earth-Retaining Structures*, Soil Mechanics and Foundations Division, ASCE, June, 1970.

31. Whitman, Robert V., "Summary of Results from Shaking Table Tests at University of Chile Using a Medium Sand," *Research Report No. R70-25*, Department of Civil Engineering, Massachusetts Institute of Technology, May, 1970.

APPENDIX II.--NOTATION

The following symbols are used in this paper:

a_{max} = maximum ground surface acceleration;
c_r = correction factor applied to results of triaxial compression tests;
D_r = relative density;
D_{50} = mean grain size;
d_w = depth of water table;
g = acceleration of gravity;
h = depth of soil element;
N = standard penetration resistance in blows per foot;
N_c = number of significant stress cycles during eqrthquake;
r_d = stress reduction coefficient;
γ = unit weight of soil;
σ_a = ambient pressure in triaxial compression test;
σ_{dc} = cyclic deviator stress;
σ'_o = effective overburden pressure;
τ = shear stress;
τ_{av} = average horizontal shear stress developed on soil element;
τ_{l10} = horizontal shear stress causing liquefaction in 10 cycles;
τ_{max} = maximum horizontal shear stress developed on soil element;
$(\tau_{max})_d$ = maximum horizontal shear stress assuming deformable body behavior; and
$(\tau_{max})_r$ = maximum horizontal shear stress assuming rigid body behavior.